A harmonized global gridded transpiration product based on collocation analysis.

Changming Li[1], Juntai Han[1], Ziwei Liu[1], Zhuoyi Tu[1], Hanbo Yang[1*]

[1]State Key Laboratory of Hydroscience and Engineering, Department of Hydraulic Engineering, Tsinghua University. Beijing 100084, China

[*]Correspondence: Hanbo Yang (yanghanbo@tsinghua.edu.cn)

Key Points

1. **Collocation Analysis for Transpiration products:** Collocation analysis rigorously evaluates errors within global transpiration products, offering insights crucial for accurate data fusion.
2. **Global Transpiration Dataset**: A daily global transpiration dataset from 2000 to 2020 at 0.1°. The merging process considers the presence of non-zero error cross correlation (ECC), theoretically and proven more effective than prior methodologies.
3. **Robust Validation:** The fused transpiration product is subjected to validation at both sites and globally. Results showcase its promising performance, demonstrating robust representation.

Abstract

Transpiration (T) is pivotal in the global water cycle, responding to soil moisture, atmospheric stress, climate changes, and human impacts. Therefore, establishing a reliable global transpiration dataset is essential. Different global transpiration products exhibit significant differences, necessitating the evaluation of errors. Collocation analysis methods have been proven effective for assessing the errors in these products, which can subsequently be used for multisource fusion. However, previous results did not consider error cross-correlation, rendering the results less reliable. In this study, we employ collocation analysis, taking error cross-correlation into account, to effectively analyze the errors in multiple transpiration products and merge them to obtain a more reliable dataset. The results demonstrate its superior reliability. The outcome of this research is a long-term daily global transpiration dataset at 0.1° resolution from 2000 to 2020. Using the transpiration after partitioning at FLUXNET sites as a reference, we compare the performance of the merged product with input datasets. The merged dataset performs well across various vegetation types and is

validated against in-situ observations. Incorporating non-zero ECC considerations represents a significant theoretical and proven enhancement over previous methodologies that neglected such conditions, highlighting its reliability in enhancing our understanding of transpiration dynamics in a changing world.

Keywords

Transpiration, Collocation analysis, Data fusions

1. Introduction

Transpiration (T) comprises approximately 60% of terrestrial evapotranspiration (ET), playing a pivotal role in Water and energy cycles (Lian et al., 2018; Wei et al., 2017). Observational records indicate a substantial warming trend over the past several decades, inducing an evident shift in soil water availability, atmospheric water stress, climate variations, and human influences, which is expected to alter transpiration (Binks et al., 2022; Keenan et al., 2016; Diego G Miralles et al., 2014; Oogathoo et al., 2022). Nevertheless, quantifying T at regional and larger scales remains an intricate challenge due to heterogeneities in the physical and physiological attributes governing plant water uptake and ecosystem water utilization (Mcgrath & Lobell, 2013; Zou et al., 2020). These challenges have resulted in limited data availability and substantial uncertainties in ecosystem T estimates, further propagating uncertainties in biosphere-atmosphere feedbacks relevant to climate change projections by Earth System models (Fisher et al., 2017; Yang et al., 2023).

Over the past decades, multiple models have emerged for estimating global T and ET. However, previous studies investigated uncertainties often exceeding two to three times those of total ET in these products (D. G. Miralles et al., 2016; Park et al., 2023; Talsma et al., 2018). Notably, substantial disparities exist among previous studies estimating global T/ET ratios, ranging from 24% to 76% based on satellite observations (D. G. Miralles et al., 2016), 31% to 64% using hydrological models

(Wei et al., 2017), and 25% to 90% derived from climate models (Berg & Sheffield, 2019). The improvement of these models is impeded by the lack of suitable datasets for direct T product validation, mechanism testing, and parameter constraints (Stoy et al., 2019). Validation efforts are often hindered by sparse in situ data (Yang et al., 2023) and the limited availability of measurement techniques and datasets at the requisite spatial and temporal scales (Bayat et al., 2021; Talsma et al., 2018).

Collocation methods have recently emerged as promising techniques for estimating random error variances and data-truth correlations in collocated inputs (C. Li et al., 2022; Xueying Li et al., 2023; Park et al., 2023; Stoffelen, 1998). These methods do not demand a high-quality reference dataset but instead rely on the availability of spatially and temporally corresponding datasets (Su et al., 2014; Wu et al., 2021). Collocation methods have found widespread application in assessing various geophysical variables, encompassing soil moisture (Deng et al., 2023; Ming et al., 2022), precipitation (Dong et al., 2022; C. Li et al., 2018), ocean wind speed (Ribal & Young, 2020; Vogelzang et al., 2022), leaf area index (Jiang et al., 2017), total water storage (Yin & Park, 2021) sea ice thickness and surface salinity (Hoareau et al., 2018), and near-surface air temperature (Sun et al., 2021).

Recent efforts have applied collocation analysis to assess transpiration estimates. Bright et al. (2022) utilized the additive triple collocation (TC) model to scrutinize the performance of diverse models in estimating daily transpiration. Park et al. (2023) amalgamated three products (e.g., ERA5L, GLDAS, and MERRA2) using TC-derived error information over East Asia. Li et al. (2023) utilized the extended double instrumental variable (EIVD) method to evaluate the uncertainty of three global gridded transpiration datasets (e.g., ERA5L, GLDAS, and GLEAM). The findings of these studies corroborated the reliability of the collocation method and highlighted its increased suitability for assessing transpiration estimates.

The mathematical premise of collocation analysis assumes that multiple products are mutually independent (Stoffelen, 1998), meaning that the random errors of these products are not correlated. If this assumption is not met, it can lead to significant errors in the results. However, in practice, many products use the same data source for driving or calibration, making it challenging to satisfy the zero ECC assumption. The subsequent developments in collocation analysis, such as extended collocation (EC) or EIVD methods, have introduced specific approaches for calculating ECC, thereby relaxing this assumption to some extent. Recent studies have demonstrated that the framework of collocation analysis can be employed for the analysis and fusion of transpiration products. However, they did not account for the potential existence of ECC, which is disadvantageous for multisource data fusion.

In summary, this study addresses the challenges posed by the difficulty in estimating global transpiration and the limited assessment of existing products. We intend to employ a collocation analysis approach considering non-zero ECC to analyze the errors in four commonly used transpiration products. Subsequently, we will perform multisource data fusion to obtain more reliable and robust global gridded transpiration data. These data will be compared with input datasets and other fusion methods at both site and global scales to assess the robustness of the fusion results. This research will provide the scientific community with reliable data support for analyzing the spatiotemporal variability trends and underlying reasons for transpiration under changing environmental conditions.

2. Datasets

In this study, we selected three global gridded vegetation transpiration datasets from 2000 to 2020 (Table 1). Additionally, we filtered a subset of sites from the global flux observation network FLUXNET and employed multiple evapotranspiration partitioning methods to calculate vegetation transpiration to comprehensively compare existing products and the performance of the fusion results. We applied Kriging spatial interpolation to downscale GLDAS-2.1 and GLEAM-3.7a from 0.25° to 0.1° and upscale PMLv2 from 0.083° to 0.1° and matched the 8-day average data to the corresponding periods, resulting in three datasets with consistent spatial and temporal resolutions for fusion.

TABLE.1 Summary of transpiration products involved.

Name	Schemes	Original Resolution (all interpolated to 0.1°)		Period
GLDAS-2.1	Noah	0.25°	3-hourly	2000-present
GLEAM-3.7a	GLEAM model	0.25°	daily	1980-2022
PMLv2-v017	Penman-Monteith-Leuning	0.083°	8-day average	2000-2020

2.1. GLDAS

The Global Land Data Assimilation System (GLDAS) product is a land-surface simulation forced by a combination of model and observation datasets incorporating advanced and sophisticated data assimilation methodologies(Rodell et al., 2004). GLDAS runs multiple land-surface models (LSMs), including Noah, Mosaic, Variable infiltration capacity (VIC), and the Community land model (CLM). These combined models provide global evapotranspiration estimations at fine and coarse spatial (0.1° and 0.25°) and temporal (3-hourly and monthly) resolutions. The latest GLDAS version 2 has three components (v2.0-v2.2). The GLDAS-2.1 started on January 2000 to present using meteorological analysis fields from ECMWF. The transpiration parameter is derived from GLDAS-2.1 products denoted as "TVeg_tavg." Transpiration is calculated as a part of total evapotranspiration using the Noah model. For more detailed descriptions of the GLDAS2 models and DA process of GLDAS-2.1, we recommend the reader refer to NASA's Hydrology Data and Information Services Center (http://disc.sci.gsfc.nasa.gov/hydrology).

2.2. GLEAM

The latest version of the Global Land Evaporation Amsterdam Model 3.7

(GLEAMv3.7) dataset(Martens et al., 2017; D Gonzalez Miralles et al., 2011) at 0.25° is used. This version of GLEAM provides daily estimations of actual evaporation, bare soil evaporation, canopy interception, transpiration from vegetation, potential evaporation, and snow sublimation from 1980 to 2022. The third version of GLEAM contains a new DA scheme, an updated water balance module, and evaporative stress functions. Two datasets that differ only in forcing and temporal coverage are provided: GLEAMv3.7a-43-year period (1980 to 2022) based on satellite and reanalysis (ECMWF) data; GLEAMv3.7b-20-year period (2003 to 2022) based on only satellite data. The cover-dependent potential evaporation rate (E_P) is calculated using the Priestley-Taylor equation(Priestley & TAYLOR, 1972). Then, a multiplicative stress factor is used to convert E_P into actual transpiration or bare soil evaporation, which is the function of microwave vegetation optimal depth (VOD) and root-zone soil moisture. For detailed description, please refer to the description paper (Martens et al., 2017).

2.3. PMLv2

The Penman-Monteith-Leuning version 2 global evaporation model (PMLv2) has been developed based on the Penman-Monteith-Leuning model(Leuning et al., 2009; Zhang et al., 2019). The daily inputs for this model include leaf area index (LAI), white sky shortwave albedo, and emissivity obtained from the Moderate Resolution Imaging Spectroradiometer (MODIS), as well as temperature variables (T_{max} , T_{min}, T_{avg}), instantaneous variables (P_{surf}, P_a, U, q), and accumulated variables (P_{rcp}, R_{ln}, R_s) from GLDAS2. Evaporation is divided into direct evaporation from bare soil (E_s), evaporation from solid water sources (water bodies, snow, and ice) (ET_{water}), and vegetation transpiration (E_c). To ensure its accuracy, the PMLv2-ET model was calibrated against 8-daily eddy covariance data from 95 global flux towers representing ten different land cover types. In this study, we employ the latest version, v017.

2.4. FLUXNET

The latest FLUXNET2015 4.0 eddy-covariance data were used in our study (Pastorello et al., 2020). Following the filtering process by Lin et al. (2018) and Li et al. (2019), only the measured and good-quality gap-filled data were used for quality control. Secondly, we excluded days with rainfall and the subsequent day after rainy events to mitigate the impact of canopy interception (Medlyn et al., 2017; Knauer et al., 2018).

After data filtering and processing, 199 sites were selected. The selected sites are distributed globally, primarily in North America and Europe. The International-Geosphere–Biosphere Program (IGBP) land cover classification system (Loveland et al., 1999) was employed to distinguish the 11 Plant Functional Types (PFTs) across sites based on the classification provided in the original dataset, including evergreen needle leaf forests (ENF, 49 sites), evergreen broadleaf forests (EBF, 13 sites), deciduous broadleaf forests (DBF, 26 sites), croplands (CRO, 20 sites), grasslands (GRA, 39 sites), savannas (SAV, 8 sites), mixed forests (MF, 8 sites), closed shrublands (CSH, 2 sites), open shrublands (OSH, 13 sites), and permanent wetland (WET, 16 sites).

3. Method

In this study, the fusion of products consisted of three steps: (1) the extended double instrumental variable technique (EIVD) was used to calculate the random error variance of the selected input products; (2) aiming for minimum MSE, the weights of different products on each grid were calculated considering non-zero error-cross-correlation (ECC); (3) the products were fused according to the weights to obtain a long sequence. In addition, to evaluate the performance of the fusion results, we employed three methods for partitioning T from ET. We calculated the means of these three methods to obtain site-scale T data for the long time series, which serves as the benchmark.

3.1. Collocation Analysis

3.1.1. Extended instrumental variable technique

The EIVD method (Dong et al., 2019) used in this study is a type of collocation analysis that combines the traditional triple collocation (TC) method (Stoffelen, 1998) with the extended collocation (EC) method (Alexander Gruber et al., 2016), which considers non-zero ECC. Therefore, we must first introduce the TC method to derive the rationale behind the EIVD method.

The commonly used error structure for triple collocation analysis (TCA) is:

$$i = \alpha_i + \beta_i \Theta + \varepsilon_i \tag{1}$$

where $i \in [X, Y, Z]$ are three spatially and temporally collocated data sets; Θ is the unknown true signal for relative geographical variable; α_i and β_i are additive and multiplicative bias factors against the true signal, respectively; ε_i is the additive zero-mean random error.

The basic assumptions adopted in TC are as follows: (i) Linearity between true signal and data sets, (ii) signal and error stationarity, (iii) independency between random error and true signal (error orthogonality), (iv) independence between random errors (zero error cross-correlation, zero ECC). Although many studies have indicated that some of these assumptions are often violated in practice (Jia et al., 2022; C. Li et al., 2018, 2022), the formulation based on these assumptions is still the most robust implementation (A. Gruber et al., 2016).

The data sets first need to be rescaled against an arbitrary reference (e.g., X). The others are scaled through a TC-based rescaling scheme:

$$Y^X = \beta_Y^X \left(Y - \overline{Y}\right) + \overline{X} \qquad Z^X = \beta_Z^X \left(Z - \overline{Z}\right) + \overline{X} \tag{2}$$

The overbar denotes the mean value, and β_Y^X and β_Z^X are the scaling factors as:

$$\begin{cases} \beta_Y^X = \dfrac{\beta_X}{\beta_Y} = \dfrac{< \left(X - \overline{X}\right)\left(Z - \overline{Z}\right) >}{< \left(Y - \overline{Y}\right)\left(Z - \overline{Z}\right) >} = \dfrac{\sigma_{XZ}}{\sigma_{YZ}} \\ \beta_Z^X = \dfrac{\beta_X}{\beta_Z} = \dfrac{< \left(X - \overline{X}\right)\left(Y - \overline{Y}\right) >}{< \left(Z - \overline{Z}\right)\left(Y - \overline{Y}\right) >} = \dfrac{\sigma_{XY}}{\sigma_{ZY}} \end{cases} \tag{3}$$

where $<\cdot>$ is the average operator, σ_{ij} is the covariance of data sets i and j. Subsequently, the error variances could be estimated by averaging the cross-multiplied data set differences as follows:

$$\begin{cases} \sigma_{\varepsilon_X}^2 =< (X - Y^X)(X - Z^X) > \\ \sigma_{\varepsilon_Y^X}^2 = {\beta_Y^X}^2 \sigma_{\varepsilon_Y}^2 =< (Y^X - X)(Y^X - Z^X) > \\ \sigma_{\varepsilon_Z^X}^2 = {\beta_Z^X}^2 \sigma_{\varepsilon_Z}^2 =< (Z^X - X)(Z^Y - Y^X) > \end{cases} \tag{4}$$

Expanding the bracket and expressing the rescaling factors yields:

$$\begin{cases} \sigma_{\varepsilon_X}^2 = \sigma_X^2 - \dfrac{\sigma_{XY}\sigma_{XZ}}{\sigma_{YZ}} \\ \sigma_{\varepsilon_Y}^2 = \sigma_Y^2 - \dfrac{\sigma_{YX}\sigma_{YZ}}{\sigma_{XZ}} \\ \sigma_{\varepsilon_Z}^2 = \sigma_Z^2 - \dfrac{\sigma_{ZX}\sigma_{ZY}}{\sigma_{XY}} \end{cases} \tag{5}$$

Following the classic TC analysis, the problem is generalized for an arbitrary number of N data sets (Zwieback et al., 2012) by relaxing the zero ECC assumption for specific data sets combination. Here, we use a quadruple input $[i, j, k, l$ with $\sigma_{\varepsilon_i\varepsilon_j} \neq 0]$for expression. The data set variances and covariances write as:

$$\sigma_{ij} = \begin{cases} \beta_i\beta_j\sigma_\Theta^2 & \forall i,j \text{ with } \sigma_{\varepsilon_i\varepsilon_j} = 0 \\ \beta_i\beta_j\sigma_\Theta^2 + \sigma_{\varepsilon_i\varepsilon_j} & \forall i,j \text{ with } \sigma_{\varepsilon_i\varepsilon_j} \neq 0 \end{cases} \tag{6}$$

The sensitivity and absolute error variance of the data set follow:

$$\beta_j^2\sigma_\Theta^2 = \frac{\sigma_{jk}\sigma_{jl}}{\sigma_{kl}} \qquad \sigma_{\varepsilon_j}^2 = \sigma_j^2 - \frac{\sigma_{jk}\sigma_{jl}}{\sigma_{kl}} \tag{7}$$

The cross-multiplied factors can be estimated by:

$$\beta_i\beta_j\sigma_\Theta^2 = \frac{\sigma_{ik}\sigma_{jl}}{\sigma_{kl}} \qquad \sigma_{\varepsilon_i\varepsilon_j} = \sigma_{ij} - \frac{\sigma_{ik}\sigma_{jl}}{\sigma_{kl}} \tag{8}$$

The above equations could be expressed in matrix notation with $\mathbf{y} = \mathbf{A}\mathbf{x}$ as:

$$\mathbf{y} = \begin{pmatrix} \sigma_i^2 \\ \sigma_{ij} \\ \dfrac{\sigma_{jl}\sigma_{jk}}{\sigma_{lk}} \\ \dfrac{\sigma_{ij}\sigma_{kl}}{\sigma_{jl}} \end{pmatrix} \quad \mathbf{A} = \begin{pmatrix} 1 & 0 & 1 & 0 \\ 0 & 1 & 0 & 1 \\ 1 & 0 & 0 & 0 \\ 0 & 1 & 0 & 0 \end{pmatrix} \quad \mathbf{x} = \begin{pmatrix} \beta_i^2 \sigma_\Theta^2 \\ \beta_i \beta_j \sigma_\Theta^2 \\ \sigma_{\varepsilon_j}^2 \\ \sigma_{\varepsilon_i \varepsilon_j} \end{pmatrix} \tag{9}$$

Where $\mathbf{y}$ is the known observations vector, $\mathbf{A}$ is the design matrix, $\mathbf{x}$ is the unknown parameters vector. The least-squared solution for unknown $\mathbf{x}$ is then solved by:

$$\mathbf{x} = (\mathbf{A}^{\mathbf{T}}\mathbf{A})^{-\mathbf{1}}\mathbf{A}^{\mathbf{T}}\mathbf{y} \tag{10}$$

The matrix $(\mathbf{A}^{\mathbf{T}}\mathbf{A})$ must have full rank (invertible) to guarantee that the collocation system is solvable. For any number of N>3, this requirement could be expressed as Each data set must be a member of at least one triplet with mutually zero ECC (Gruber et al., 2016a). For example, input with five data sets $[a, b, c, d, e]$ can assume at most 2 sets with 2 non-zero ECC pairs (like $\sigma_{\varepsilon_a \varepsilon_b} \& \sigma_{\varepsilon_a \varepsilon_c} \neq 0$ and $\sigma_{\varepsilon_a \varepsilon_b} \& \sigma_{\varepsilon_c \varepsilon_d} \neq 0$) or $\mathrm{C}_5^2 = 10$ sets with 1 non-zero ECC pair, etc.

The instrumental variable algorithm introduces a temporally lag-1 [day] series of the select product (e.g., $X_{t-1} = \alpha_X + \beta_X \Theta_{t-1} + \varepsilon_{X,t-1}$) as the third input for TC (Su et al., 2014). Such process includes another assumption that all data sets contain serially white errors (i.e., $< \varepsilon_{i,t}\varepsilon_{i,t-1} >= 0$, zero auto-correlation). Furthermore, by adopting the designed matrix in extended collocation (EC) (Alexander Gruber et al., 2016), Dong et al. (2020) present the extended double instrumental variable technique (denoted as EIVD) to estimate the error variance matrix with only two independent data sets.

For a triplet input $\left[i, j, k \text{ with } \sigma_{\varepsilon_i \varepsilon_j} \neq 0\right]$. The dynamic range ratio scaling factors can be estimated as follows:

$$s_{ij} \equiv \frac{\beta_i}{\beta_j} = \sqrt{\frac{L_{ii}}{L_{jj}}} \tag{11}$$

where $L_{ii} =< i_t i_{t-1} >$ is the auto-covariance of inputs. Subsequently, the sensitivity and absolute error variance of the data set follow:

$$\beta_j^2\sigma_\Theta^2 = \sigma_{ij}\sqrt{\frac{L_{ii}}{L_{jj}}} \qquad \sigma_{\varepsilon_j}^2 = \sigma_{ij}\sqrt{\frac{L_{ii}}{L_{jj}}} - \sigma_i^2 \tag{12}$$

The cross-multiplied factors can be estimated by:

$$\beta_i\beta_j\sigma_\Theta^2 = \sigma_{ik}\sqrt{\frac{L_{jj}}{L_{kk}}} = \sigma_{jk}\sqrt{\frac{L_{ii}}{L_{kk}}} \quad \sigma_{\varepsilon_i\varepsilon_j} = \sigma_{ij} - \beta_i\beta_j\sigma_\Theta^2 \tag{13}$$

Hence, for a triplet with the input of $[X, Y, Z$ with $\sigma_{\varepsilon_X\varepsilon_Y} \neq 0]$: the matrix notation of the above system with $\mathbf{y} = \mathbf{Ax}$ is given as:

$$\mathbf{y} = \begin{pmatrix} \sigma_X^2 \\ \sigma_Y^2 \\ \sigma_Z^2 \\ \sigma_{XY} \\ \sigma_{XZ}\sqrt{\frac{L_{XX}}{L_{ZZ}}} \\ \sigma_{YZ}\sqrt{\frac{L_{YY}}{L_{ZZ}}} \\ \sigma_{ZX}\sqrt{\frac{L_{ZZ}}{L_{XX}}} \\ \sigma_{ZY}\sqrt{\frac{L_{ZZ}}{L_{YY}}} \\ \sigma_{XZ}\sqrt{\frac{L_{YY}}{L_{ZZ}}} \\ \sigma_{YZ}\sqrt{\frac{L_{XX}}{L_{ZZ}}} \end{pmatrix}_{\mathbf{10x1}} \quad \mathbf{A} = \begin{pmatrix} \mathbf{I_{4x4}} & \mathbf{I_{4x4}} \\ \begin{pmatrix} 1 & 0 & 0 & 0 \\ 0 & 1 & 0 & 0 \\ 0 & 0 & 1 & 0 \\ 0 & 0 & 1 & 0 \\ 0 & 0 & 0 & 1 \\ 0 & 0 & 0 & 1 \end{pmatrix}_{\mathbf{6x4}} & \mathbf{0_{6x4}} \end{pmatrix}_{\mathbf{10x8}} \quad \mathbf{x} = \begin{pmatrix} \beta_X^2\sigma_\Theta^2 \\ \beta_Y^2\sigma_\Theta^2 \\ \beta_Z^2\sigma_\Theta^2 \\ \beta_X\beta_Y\sigma_\Theta^2 \\ \sigma_{\varepsilon_X}^2 \\ \sigma_{\varepsilon_Y}^2 \\ \sigma_{\varepsilon_Z}^2 \\ \sigma_{\varepsilon_X\varepsilon_Y} \end{pmatrix}_{\mathbf{8x1}} \tag{14}$$

Likewise, the least-squared solution for unknown **x** is solved by Eq (10).

3.1.2. Weight Estimation

Our objective is to predict an uncertain variable, such as transpiration (ET) over time at a specific location, by utilizing parent products that may contain random errors. The underlying concept of weighted averaging is to extract independent information from multiple data sources to enhance prediction accuracy by mitigating the effects of random errors. The effectiveness of this approach relies on the independence of the individual data sources. Weighted averaging has been applied in various fields following the influential work of Bates and Granger (1969), which proposed the optimal combination of forecasts based on a mean square error (MSE) criterion. In this context, the term "optimal" refers to minimizing the variance of residual random errors in the least squares sense. Mathematically, this weighted average can be expressed as follows:

$$\overline{x} = \vec{\mathbf{W}}^{\mathrm{T}}\vec{\mathbf{X}} = \sum_{i=1}^{N} \omega_i x_i \tag{15}$$

where $\overline{x}$ is the merged estimate; $\vec{\mathbf{X}} = [x_1, \dots, x_n]^{\mathrm{T}}$ contains the temporally collocated estimates from N different parent products, which are merged with relative zero-mean random error $\vec{\boldsymbol{e}} = [\varepsilon_1, \dots, \varepsilon_n]^{\mathrm{T}}$; and $\vec{\mathbf{W}} = [\omega_1, \dots, \omega_n]^{\mathrm{T}}$ contains the weights assigned to these estimates, where $\omega_i \in [0,1]$ and $\sum \omega_i = 1$ ensuring an unbiased prediction. The averaging weights can be expressed as the solution to the problem:

$$\min f\left(\vec{\mathbf{W}}\right) = \mathbb{E}\left(\vec{\boldsymbol{e}}^{\mathrm{T}}\vec{\mathbf{W}}\right)^2 \tag{16}$$

where $\mathbb{E}()$ is the operator for mathematical expectation, the solution of this problem is determined by the individual random error characteristics of the input data sets and can be derived from their covariance matrix (Bates & Granger, 1969; Alexander Gruber et al., 2017; Kim et al., 2021):

$$\begin{gathered} \vec{\mathbf{W}} = \left(\vec{\mathbf{I}}^{\mathrm{T}}\mathbb{E}(\vec{\boldsymbol{e}}\vec{\boldsymbol{e}}^{\mathrm{T}})^{-1}\vec{\mathbf{I}}\right)^{-1}\mathbb{E}(\vec{\boldsymbol{e}}\vec{\boldsymbol{e}}^{\mathrm{T}})^{-1}\vec{\mathbf{I}} \\ \sigma_{\varepsilon_{\overline{x}}}^2 = \left(\vec{\mathbf{I}}^{\mathrm{T}}\mathbb{E}(\vec{\boldsymbol{e}}\vec{\boldsymbol{e}}^{\mathrm{T}})^{-1}\vec{\mathbf{I}}\right)^{-1} \end{gathered} \tag{17}$$

where $\mathbb{E}(\vec{\boldsymbol{e}}\vec{\boldsymbol{e}}^{\mathrm{T}})$ is the $N \times N$ error covariance matrix that holds the random error variance $\sigma_{\varepsilon_i}^2$ of the parent products in the diagonals and relative error covariances $\sigma_{\varepsilon_i\varepsilon_j}$ in the off-diagonals; $\vec{\mathbf{I}} = [1, \dots, 1]^{\mathrm{T}}$ is an ones-vector of length N; and $\sigma_{\varepsilon_{\overline{x}}}^2$ is the resulting random error variances of the merged estimate.

When only two groups of products are used as input ($N = 2$), it is generally assumed that the errors between them are independent. In this case, the weights are as follows:

$$\mathbb{E}(\vec{\boldsymbol{e}}\vec{\boldsymbol{e}}^{\mathrm{T}}) = \begin{bmatrix} \sigma_{\varepsilon_1}^2 & 0 \\ 0 & \sigma_{\varepsilon_2}^2 \end{bmatrix}$$
$$\omega_1 = \frac{\sigma_{\varepsilon_2}^2}{\sigma_{\varepsilon_1}^2 + \sigma_{\varepsilon_2}^2} \qquad \omega_1 = \frac{\sigma_{\varepsilon_1}^2}{\sigma_{\varepsilon_1}^2 + \sigma_{\varepsilon_2}^2} \tag{18}$$

In most cases, we can identify three sets of products as inputs ($N = 3$). In this scenario, we consider the possibility of error homogeneity, assuming a non-zero ECC exists between inputs 1 and 2. In this case, the error matrix can be represented as:

$$\mathbb{E}(\vec{\boldsymbol{e}}\vec{\boldsymbol{e}}^{\mathrm{T}}) = \begin{bmatrix} \sigma_{\varepsilon_1}^2 & \sigma_{\varepsilon_1\varepsilon_2} & 0 \\ \sigma_{\varepsilon_1\varepsilon_2} & \sigma_{\varepsilon_2}^2 & 0 \\ 0 & 0 & \sigma_{\varepsilon_3}^2 \end{bmatrix} \tag{19}$$

The weights can then be written as:

$$\vec{\mathbf{W}} = \begin{cases} \dfrac{\sigma_{\varepsilon_2}^2 - \sigma_{\varepsilon_1\varepsilon_2}}{\left(\sigma_{\varepsilon_1}^2\sigma_{\varepsilon_2}^2 - \sigma_{\varepsilon_1\varepsilon_2}^2\right) * \mathbb{Z}} \\ \dfrac{\sigma_{\varepsilon_1}^2 - \sigma_{\varepsilon_1\varepsilon_2}}{\left(\sigma_{\varepsilon_1}^2\sigma_{\varepsilon_2}^2 - \sigma_{\varepsilon_1\varepsilon_2}^2\right) * \mathbb{Z}} \\ \dfrac{1}{\sigma_{\varepsilon_3}^2 * \mathbb{Z}} \end{cases}$$
$$\mathbb{Z} = \frac{\sigma_{\varepsilon_1}^2 + \sigma_{\varepsilon_2}^2 - 2\sigma_{\varepsilon_1\varepsilon_2}}{\sigma_{\varepsilon_1}^2\sigma_{\varepsilon_2}^2 - \sigma_{\varepsilon_1\varepsilon_2}^2} + \frac{1}{\sigma_{\varepsilon_3}^2} \tag{20}$$

It is essential to acknowledge that before applying these weights for merging the data sets, it is necessary to address any existing systematic differences. Typically, this is achieved by rescaling the data sets to a standardized data space. Consequently, the weights can be derived from the rescaled data sets using Eq (2)-(3) and converge accordingly. This procedure ensures the accuracy and reliability of the merged data sets for further analysis.

If ECC is not considered (i.e., setting $\sigma_{\varepsilon_1\varepsilon_2} = 0$), Eq (20) represents the weight calculation method commonly used in most TC fusion studies. This method was initially applied by Yilmaz et al.(2012) in the fusion of multisource soil moisture products and later improved by Gruber et al. (2017) and further applied in the production of the ESA CCI global soil moisture product (Alexander Gruber et al., 2019). Dong et al. (2020b) also adopted this approach to fusing multisource precipitation products. In the study of evapotranspiration, Li et al. (2023) and Park et al.(2023) utilized a weight calculation method that does not consider non-zero ECC and fused multiple ET products in the Nordic and East Asia, respectively, achieving satisfactory fusion results.

In contrast to the fusion studies mentioned above, the consideration of non-zero ECC is incorporated into the fusion process and the weight calculation. Yilmaz and Crow (2014) have demonstrated that TC underestimates error variances when the zero ECC assumption is violated. Li et al. (2023), in their evaluation study of global transpiration products using the collocation method, also indicated the existence of error homogeneity issues between commonly used products (such as GLDAS and GLEAM), necessitating the consideration of the influence of non-zero ECC. The merging technique employed in this study provides a more explicit characterization of product errors and facilitates the derivation of more reliable weight coefficients, thereby achieving superior fusion outcomes.

The differences in results are evaluated at the site scale by contrasting the scenarios without considering non-zero ECC and directly using simple averages to compare and validate the advantages of the weight calculation method used in our study.

3.2. Partition method

In this study, we applied three distinct methodologies to estimate transpiration (T) from eddy covariance (EC) datasets: (i) the water use efficiency (uWUE) method (Zhou et al., 2016); (ii) the Pérez-Priego method (Perez-Priego et al., 2018); (iii) the Transpiration Estimation Algorithm (TEA) method (Jacob A Nelson et al., 2018). Each of these methods provides unique insights into this crucial component of the terrestrial water cycle. We calculated the average values of these three partition methods to serve as benchmarks for validating site-scale fusion results.

These three methods exhibit disparities in their assumptions, structural design, and conceptualization disparities. These disparities encompass aspects such as the number of parameters employed (one or two in uWUE, depending on the temporal scale, versus four in Pérez-Priego), parametric versus nonparametric approaches (uWUE and Pérez-Priego versus TEA), the assumption that transpiration (T) is approximately equal to evapotranspiration (ET) for some portion of the data (uWUE and TEA versus Pérez-Priego), and the inclusion of physiological parameters characterizing leaf carbon-water optimality (Pérez-Priego and uWUE versus TEA).

Our selection of these methods was deliberate, as they are specifically designed to harness contemporary EC datasets, such as those provided by FLUXNET and its associated regional networks. These datasets are valuable due to their continuous measurements of critical variables, including CO_2 concentrations, sensible heat flux, latent heat flux, and meteorological parameters. These variables are recorded at half-hourly or hourly intervals. Leveraging this wealth of data, all three methods rely on estimates of Gross Primary Productivity (GPP) to partition total evapotranspiration (ET) into its constituent components, namely, evaporation (E) and transpiration (T). This partitioning is founded on the fundamental principle that the uptake of CO_2 and the loss of water vapor through transpiration are intricately linked processes regulated by stomatal conductance in higher plants (Cowan & GD, 1977).

It is essential to acknowledge the existence of alternative approaches for ET partitioning (Xi Li et al., 2019; Stoy et al., 2019). While these alternative methods offer valuable tools for specialized applications, they were not subjected to detailed examination within the scope of this investigation.

3.2.1. The underlying water use efficiency (uWUE) method

The uWUE method, which is the simplest of the three methods to calculate, relies on estimates of the $uWUE$, defined as,

$$uWUE = \frac{GPP \times \sqrt{VPD}}{ET} \tag{21}$$

Where VPD is the vapor pressure deficit, we have computed two variants of the uWUE metric using half-hourly data: (a) potential $uWUE_p$, determined at an annual scale by establishing a 95th percentile regression relationship between GPP×√VPD and ET. This variant characterizes conditions where the carbon gain is maximized relative to water loss, leading to T≈ET; (b) apparent $uWUE_a$, which is derived as the linear regression slope within a moving window spanning either one or eight days or directly from Equation (21) when estimating at a half-hourly resolution, contingent on the desired smoothing level and data availability. In the case of $uWUE_p$, it is assumed to remain constant throughout the year, aligning with the notion of maximum carbon gain to water loss, as demonstrated across a diverse range of sites and associated with stomatal optimality (Lin et al., 2018). T/ET is then estimated as:

$$\frac{T}{ET} = \frac{uWUE_a}{uWUE_p} \tag{22}$$

3.2.2. The Pérez-Priego method

The Pérez-Priego method (Perez-Priego et al., 2018) employs a comprehensive "big leaf" model incorporating four distinct parameters within a 5-day moving window. These parameters are intricately linked to the response of canopy conductance to vapor pressure deficit (VPD), photosynthetically active radiation (PAR), and temperature. Additionally, they govern the response of the maximum photosynthetic rate to VPD and ambient CO2 levels. A notable aspect of this method is its incorporation of the leaf optimality concept, wherein the maximization of carbon gain relative to water loss is a central objective. This is achieved by integrating a penalty mechanism within the cost function for parameters that yield suboptimal leaf carbon-water optimality.

The Pérez-Priego method presents a practical and physiologically grounded framework for partitioning water fluxes. It holds considerable applicability across diverse flux measurement sites, biomes, and plant functional types. Notably, this approach is a valuable complement to long-term flux measurements such as those obtained through FLUXNET. An additional advantage of this method lies in its capacity to unveil the underlying mechanisms driving plants to adapt and exhibit distinct behaviors under varying environmental conditions.

3.2.3. The transpiration estimation algorithm (TEA) method

The TEA method (Jacob A Nelson et al., 2018) employs a nonparametric modeling approach, leveraging the random forest technique to forecast Water Use Efficiency (WUE), denoted as the ratio of Gross Primary Productivity (GPP) to Transpiration (T). This modeling framework is trained on ecosystem-level WUE (WUE_{eco}), the ratio of GPP to Evapotranspiration (ET), specifically during periods within the growing season and under conditions where surfaces are anticipated to dry, indicates minimal E/ET ratios. The model employs a filtering process based on precipitation input and ET values calculated within a shallow bucket water balance scheme to identify periods characterized by wet surfaces. Subsequently, the random forest model, trained on WUE_{eco} data derived from the filtered periods, is applied to predict WUE values for the entire time series under investigation:

$$WUE_{TEA} = RF(R_g, T_{air}, RH, CSWI, GPP, \dots) \quad (23)$$

Where R_g is the incoming radiation, T_{air} is the air temperature, $CSWI$ is the conservative surface wetness index. GPP and $Tair$ filters were designed to ensure plants are active while R_g filters remove nighttime values. The $CSWI$ filter attempts to remove periods where the surface is likely wet. A critical aspect of our methodology is the selection of the 75th percentile as the optimal prediction percentile. This choice was based on rigorous evaluation against synthetic data generated by three terrestrial biosphere models, demonstrating its superior performance.

3.2.4. Application of partition methods

The three methods were implemented using the Python code generously provided by Nelson et al. (2020), which is accessible in the associated repository located at https://github.com/jnelson18/ecosystem-transpiration, complete with a tutorial. Our approach for the uWUE method involved estimating uWUEp annually and deriving uWUEa using an 8-day moving window. In the case of the Pérez-Priego method, we performed daily parameter optimization using a 5-day moving window, which was designed to contain high-quality data. The TEA method was applied per the procedure outlined in Nelson et al. (2018).

It is worth highlighting that the estimation procedure employed for the Pérez-Priego method did not consistently yield satisfactory solutions for the parameters. Consequently, this occasionally resulted in erratic values for transpiration, thereby impeding the generation of continuous T estimates. In contrast, more extensive and robust T estimations were obtainable through the TEA and uWUE methods. As a result, we relied on the average values produced by all three methods, acknowledging that there were periods during which only the TEA and uWUE methods were applicable. This averaged dataset served as the benchmark against which we evaluated the performance of the merged results.

3.3. Evaluation indices

Five statistical indicators, namely Root-mean-squared-error ($RMSE$), Pearson's correlation coefficient (R), Mean-absolute-error (MAE), unbiased $RMSE$ ($ubRMSE$) and Kling-Gupta Efficiency (KGE), are selected for comparison with existing products. The relative equations are shown as follows:

$$RMSE = \sqrt{\frac{\sum_{i=1}^{n}(sim_i - obs_i)^2}{n}} \tag{24}$$

$$R = \frac{\sum_{i=1}^{n}\left(sim_i - \overline{sim}\right)\left(obs_i - \overline{obs}\right)}{\sqrt{\sum_{i=1}^{n}\left(sim_i - \overline{sim}\right)^2 \sum_{i=1}^{n}\left(obs_i - \overline{obs}\right)^2}} \tag{25}$$

$$-1 \leq R \leq 1$$

$$MAE = \frac{1}{n}\sum_{i=1}^{n}|sim_i - obs_i| \tag{26}$$

$$ubRMSE = \sqrt{\frac{\sum_{i=1}^{n}\left[\left(sim_i - \overline{sim}\right) - \left(obs_i - \overline{obs}\right)\right]^2}{n}} \quad (27)$$

Where sim is the simulations, obs is the observation as reference.

The modified KGE (Kling et al., 2012) addressed several shortcomings in Nash-Sutcliffe Efficiency (NSE) and are increasingly used for calibration and evaluation (Knoben et al., 2019), given by:

$$KGE = 1 - \sqrt{(r-1)^2 + (\beta-1)^2 + (\gamma-1)^2} \quad (28)$$

Where r is the correlation coefficient between simulation and observation, $\beta = \frac{\sigma_{obs}}{\sigma_{sim}}$ is the bias ratio (dimensionless), $\gamma = \frac{CV_s}{CV_o} = \frac{\sigma_{sim}/\mu_{sim}}{\sigma_{obs}/\mu_{obs}}$ is the variability ratio (dimensionless), μ is the mean, and σ is the standard deviation. Similar to NSE, KGE = 1 indicates perfect agreement of simulations, while $KGE < 0$ reveals that the average of observations is better than simulations (Kling et al., 2012; Towner et al., 2019).

4. Results

In this study, we aimed to meticulously assess the performance of fused products at both site-specific and global scales. We evaluated the fused products at the site level by comparing them against mean transpiration (T) estimates obtained through three partitioning methods at selected FLUXNET sites. These assessments were further juxtaposed with other product variants, including simple averages and conditions that omitted considering non-zero eddy covariance correction (ECC). We scrutinized the spatial variations in land surface transpiration computed by the fused products globally, drawing comparisons with input results.

4.1. EIVD-based error analysis

We first analyzed the random error variance of the input products computed using the EIVD method. Here, we assumed a scenario where random errors were homoscedastic between GLDAS and GLEAM. The remaining potential ECC scenarios were also calculated using the EIVD method and were analyzed in the discussion section.

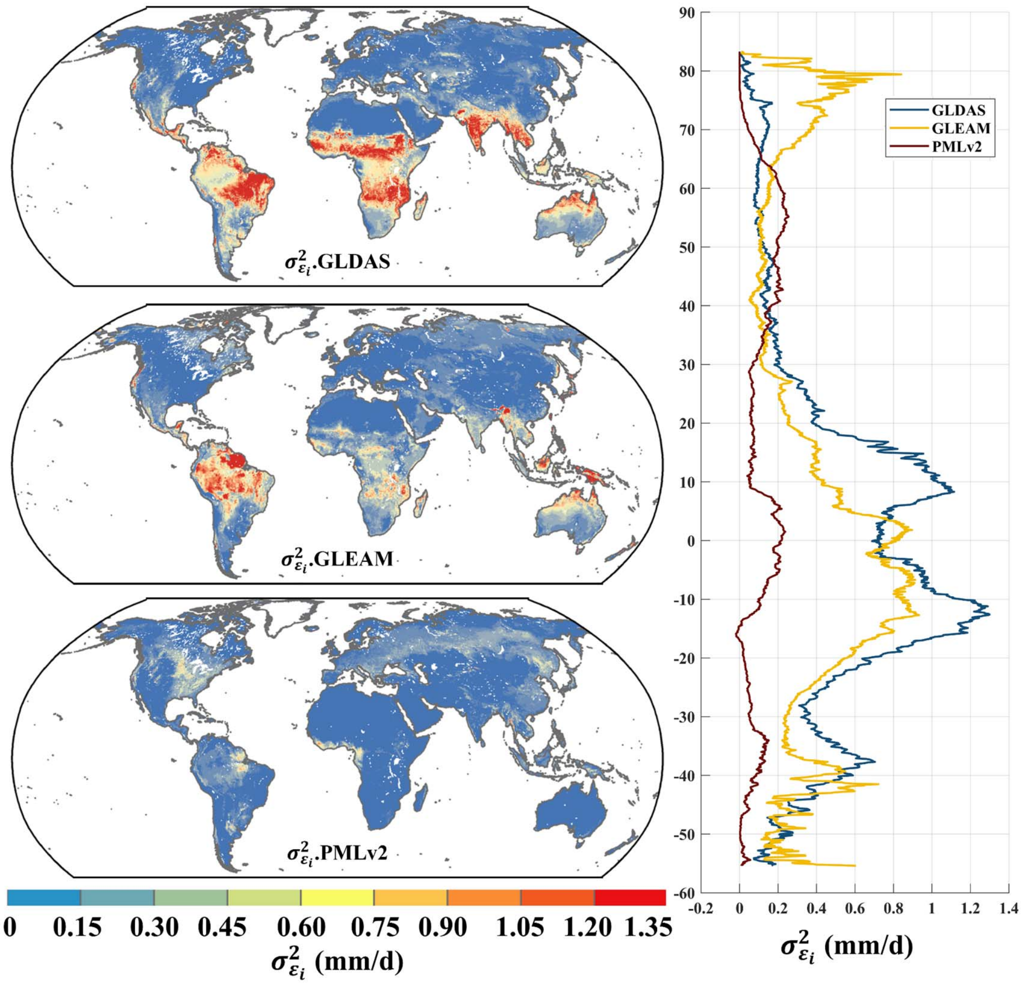

FIGURE.1 Global distribution of random error variances ($\sigma^2_{\varepsilon_i}$) of GLDAS, GLEAM, and PMLv2 using EIVD at 0.1° from 2000 to 2000, depicted alongside corresponding variation curves of average with latitude.

Figure 1 depicts the random errors of the products calculated using the EIVD method from 2000 to 2020 at 0.1°, where a non-zero ECC is assumed between GLDAS and GLEAM. The global random error variances (mean ± standard deviation) obtained using the EIVD method were as follows: GLDAS: 0.36 ± 0.43 mm/day, GLEAM: 0.29 ± 0.35 mm/day, PMLv2: 0.13 ± 0.16 mm/day. These results indicated that PMLv2 performed best overall, while GLDAS performed the poorest. Regarding the global spatial distribution, GLDAS exhibited high random errors in Central South America, Southern Africa, Southeast Asia, and South Asia. GLEAM similarly showed poorer performance in Central South America and Indonesia.

In contrast, PMLv2 demonstrates minor errors on a global scale, particularly excelling in the Amazon region. Li et al. (2023) analyzed the performance of GLDAS and GLEAM at a 0.25° resolution using the EIVD method. Although they employed different triplets to calculate the EIVD results, the spatial distribution of random errors for GLDAS and GLEAM obtained in their study were similar, indicating that GLDAS exhibits more significant errors than others.

The latitudinal distribution revealed that overall, PMLv2 outperformed GLEAM and GLDAS. There could be two reasons for this phenomenon: (1) PMLv2 employed a transpiration calculation model that considered vegetation stomatal conductance, offering a more physically grounded approach. Additionally, it utilized observational data from flux stations for calibration and correction, providing a more robust physical basis (Zhang et al., 2019); (2) In this study, the data from GLDAS and GLEAM were interpolated from 0.25° to 0.1°, which involves a straightforward statistical downscaling process that may introduce some uncertainty. This aspect will be discussed further in the subsequent sections.

4.2. Site-scale evaluation

At the site scale, this study used the average transpiration values calculated using three different ET partitioning methods as benchmarks to evaluate the performance of the fused products. Simultaneously, the results were compared between three input data sets and TC-merged results (without considering non-zero ECC conditions). Figure 2 corresponds to Table 2, where statistical parameters were computed by pooling data from all sites. Similarly, Figure 3 corresponds to Table 3, where statistical parameters were computed separately for each site and then analyzed.

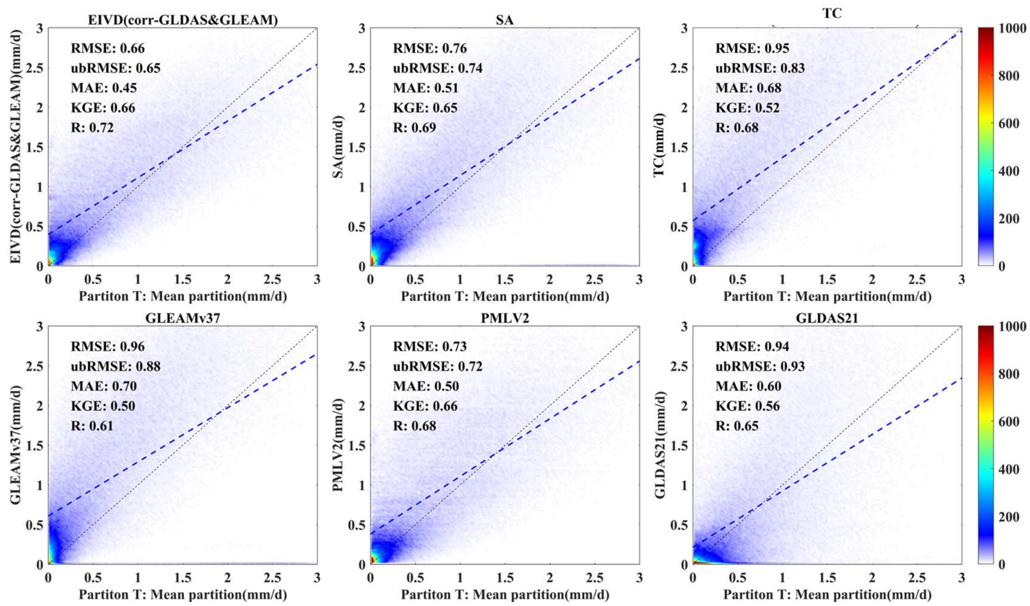

FIGURE.2 Scatter plots of products corresponding to the available period data from FLUXNET sites. The color bar represents the density, with darker colors indicating higher concentration, with "SA" indicating the results based on the simple average.

The findings depicted in Figure 2 underscored the enhanced accuracy achieved by the EIVD method in transpiration estimation through fusion. Notably, the fusion outcomes exhibited marked improvements across multiple parameters compared to three sets of products. These improvements were evident in correlation metrics, where the Pearson coefficient for the fusion results reached 0.72, and the KGE registered at 0.66, surpassing the input data's performance. Error metrics also reflected these advancements, with the fusion results displaying lower RMSE, ubRMSE, and MAE values than the input datasets. These findings indicated that applying the EIVD method in fusion effectively mitigated errors associated with the inputs, resulting in more promising outcomes.

Furthermore, when comparing the results of the EIVD method with those of the Simple Average (SA) and TC fusion methods, all three fusion approaches exhibited enhancements in correlation metrics (as indicated by KGE and R). However, the EIVD method notably reduced errors, including RMSE and other measures. EIVD fusion results were superior to TC fusion results, suggesting that considering non-zero

ECC was meaningful for fusion based on collocation analysis. Additionally, while the SA method could achieve decent fusion results, it was observed that a significant portion of points clustered around the x-axis. This clustering phenomenon may be attributed to the prevalence of estimation values close to zero in GLDAS or GLEAM. Consequently, these findings indicate that the SA method did not emerge as the optimal fusion approach in this study, with the EIVD method proving to be a more reliable alternative.

Table.2 Average values of different metrics. The bolded sections indicate the results with the best performance in their respective metrics.

Product		RMSE (mm/d)	ubRMSE (mm/d)	MAE (mm/d)	KGE	R
0.1°-daily	**EIVD-Merged**	**0.66**	**0.65**	**0.45**	**0.66**	**0.72**
	TC-Merged	0.95	0.83	0.68	0.52	0.68
	SA	0.76	0.74	0.51	0.65	0.69
	GLDAS21	0.94	0.93	0.60	0.56	0.65
	GLEAMv3.7a	0.96	0.88	0.70	0.50	0.61
	PMLv2.017	0.73	0.72	0.50	0.66	0.68

The information in Table 2 corresponded to Figure 2, with the bolded sections corresponding to the products that performed the best in their respective statistical metrics. The results indicated that the fused data obtained in this study showed strong performance across various indicators at the site scale when averaging using three ET partition methods as a benchmark. Furthermore, the performance of PMLv2 was notably impressive. Although this product solely used FLUXNET data for ET correction (Zhang et al., 2019), it theoretically enhanced its transpiration estimation, which could potentially explain the strong performance observed in the PMLv2 product.

Figure 3 corresponds to Table 4. Statistical parameters were computed separately for each site, and the results were used to generate violin graphs. Our findings demonstrated that, within the scope of this study, the fused transpiration product consistently outperformed the three sets of inputs, as well as the simple average (SA) and TC methods, across a diverse range of performance metrics. Regarding correlation metrics, the fused product exhibited higher KGE scores than the other products and combinations. While the R index was slightly lower when compared to the PMLv2 method, this aligned with the observed trends in Figure 3. When examining error metrics, the fused results consistently exhibited superior performance, thus reinforcing the conclusion that the EIVD-based fusion method, accounting for non-zero ECC, effectively mitigated errors in transpiration estimation.

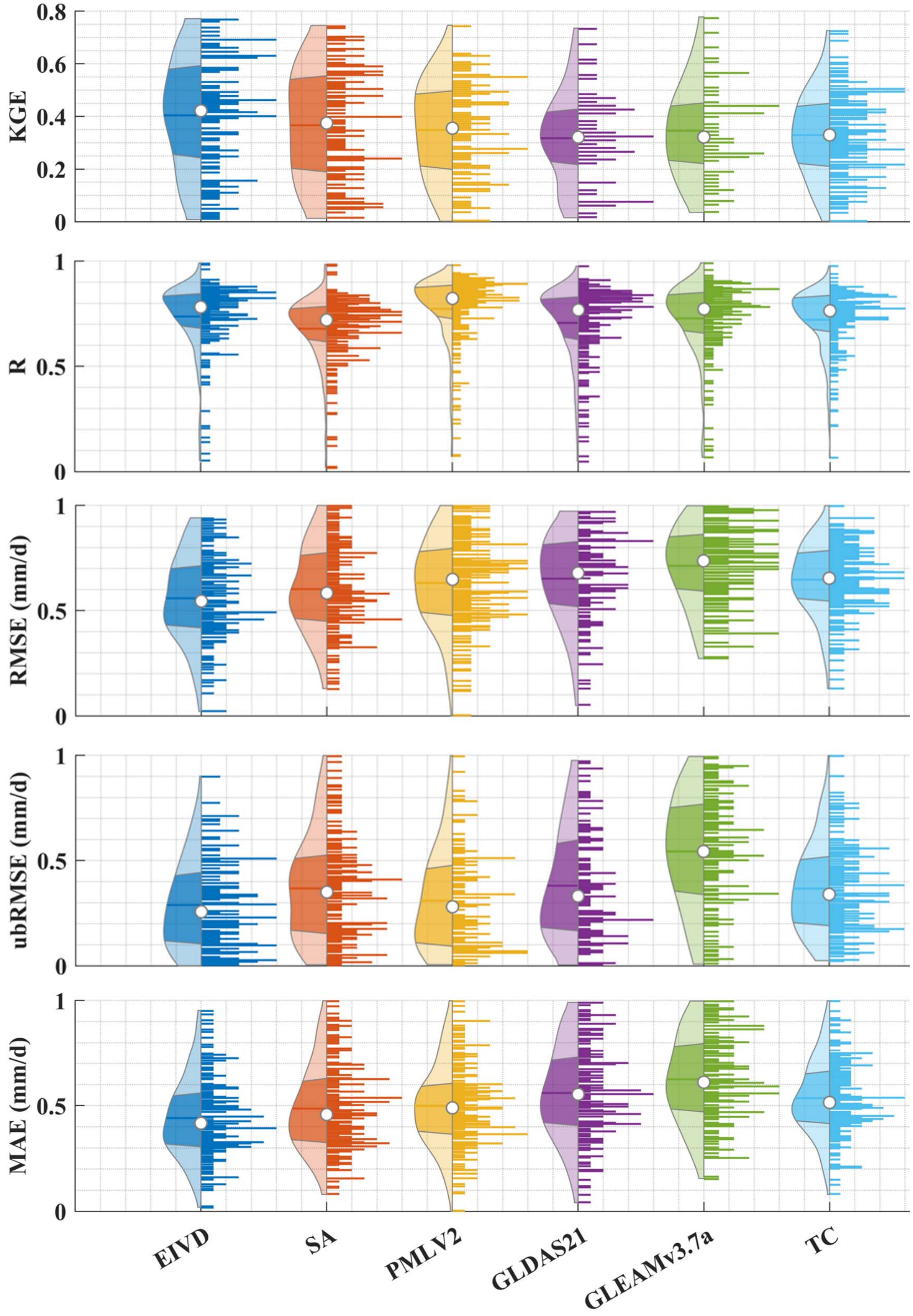

Figure.3 Violin plots obtained by aggregating five different statistical indicators, calculated separately for each site. In each violin plot, the left side represents the distribution, with the shaded area indicating the box plot, the dot representing the

mean, and the right side showing the histogram.

Table.3 Average values of indicators corresponding to different products, calculated based on the comprehensive results obtained for each site. The bolded sections indicate the schemes with the best performance in their respective metrics.

Product		**RMSE (mm/d)**	**ubRMSE (mm/d)**	**MAE (mm/d)**	**KGE**	**R**
0.1°-daily	**EIVD-Merged**	**0.56**	**0.29**	**0.44**	**0.40**	0.74
	TC-Merged	0.65	0.37	0.56	0.33	0.72
	SA	0.60	0.38	0.49	0.37	0.68
	GLDAS21	0.71	0.31	0.62	0.32	0.71
	GLEAMv3.7a	0.65	0.37	0.54	0.36	0.73
	PMLv2.017	0.63	0.54	0.50	0.35	**0.77**

Table 3 presents the average results of different statistical indicators, with the corresponding optimal products highlighted in bold. The fusion results demonstrated promising performance across all indicators, especially in reducing overall errors, as indicated by the error metrics.

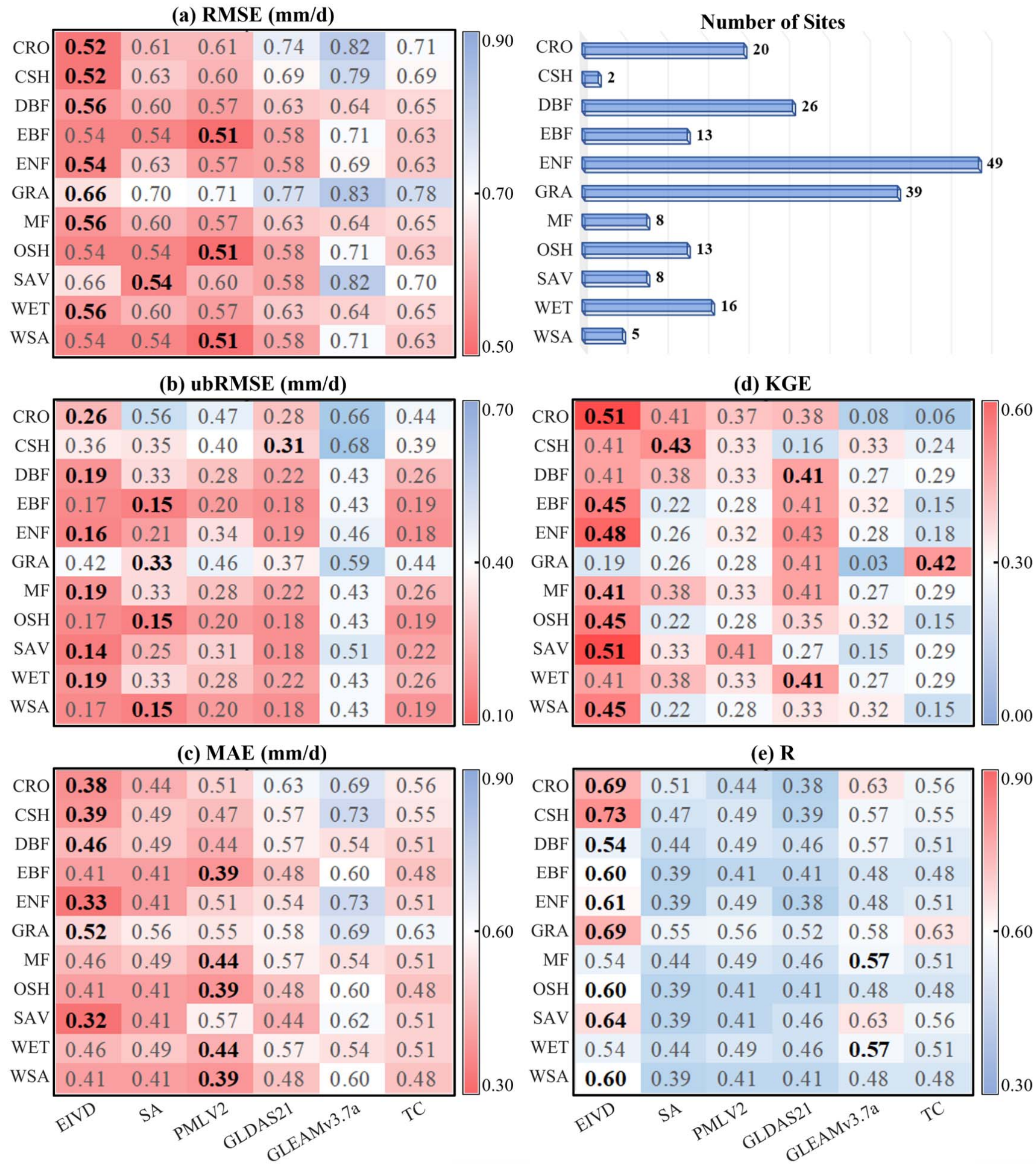

Figure.4 Average value of five statistical indicators for FLUXNET sites classified by PFTs. Each row represents the value for the merged product, simple-averaged (SA) result, three input datasets and TC-based results at relative sites with the same PFT. The bold value indicates the best performance for the relative indicator.

Additionally, we calculated statistical parameter averages for sites with the same PFTs based on information from 199 FLUXNET site data sources and generated a heatmap, as shown in Figure 4. The results showed that the merged product performed the best in almost all PFT categories, as indicated by various indicators. While on sites where other products performed better, merged-product indicators were comparable to the optimal products, albeit slightly inferior. This indicated that our fusion approach effectively combined the advantages of different products, resulting in superior fusion results across different vegetation types.

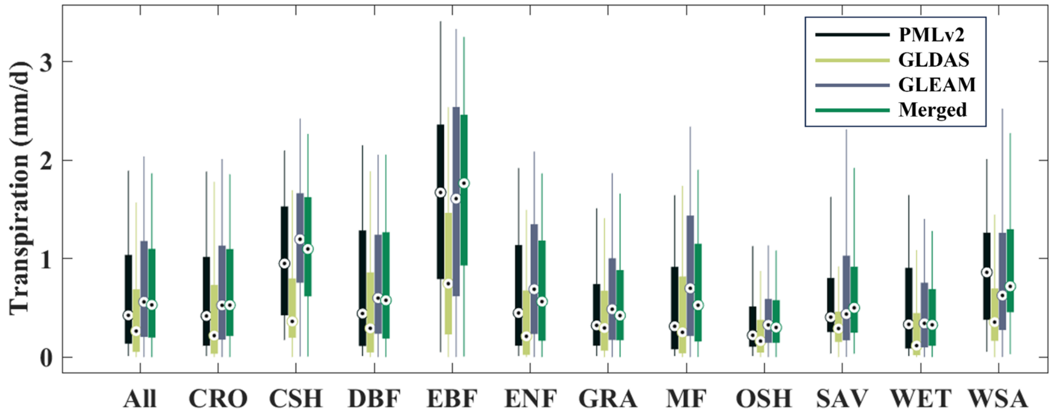

Figure.5 Box plots of daily transpiration estimates of three input datasets and the merged product at the same PFT sites from 2000 to 2020.

The estimation results of different products at the same PFT site were further analyzed. It can be observed that GLDAS consistently showed lower values compared to PMLv2 and GLEAM at all sites, especially at EBF and CSH sites, with the median values differing by more than twice. The fused results obtained in this study generally fall between PMLv2 and GLEAM at most sites, with relatively higher values at EBF sites. There are significant differences among the different products.

In summary, our study, founded on the computation of average transpiration values through three distinct ET partitioning methods across 199 FLUXNET sites, entailed a comprehensive benchmark analysis of the merged outcomes. This analysis convincingly established the robust alignment of our merged results with the reference data. Furthermore, through meticulous product performance comparisons at each site, we underscored the accuracy and minimal errors associated with our merged results. These findings highlighted that our merged outcomes consistently exhibited equivalent or slightly enhanced precision compared to existing products, including those grounded in simple averaging techniques and TC-merged approaches.

4.3. Global comparison

This section compared multi-year average daily transpiration distributions at 0.1° between the merged results and alternative products. The presented results were derived from calculations utilizing data from 2000 to 2020 to ensure consistency.

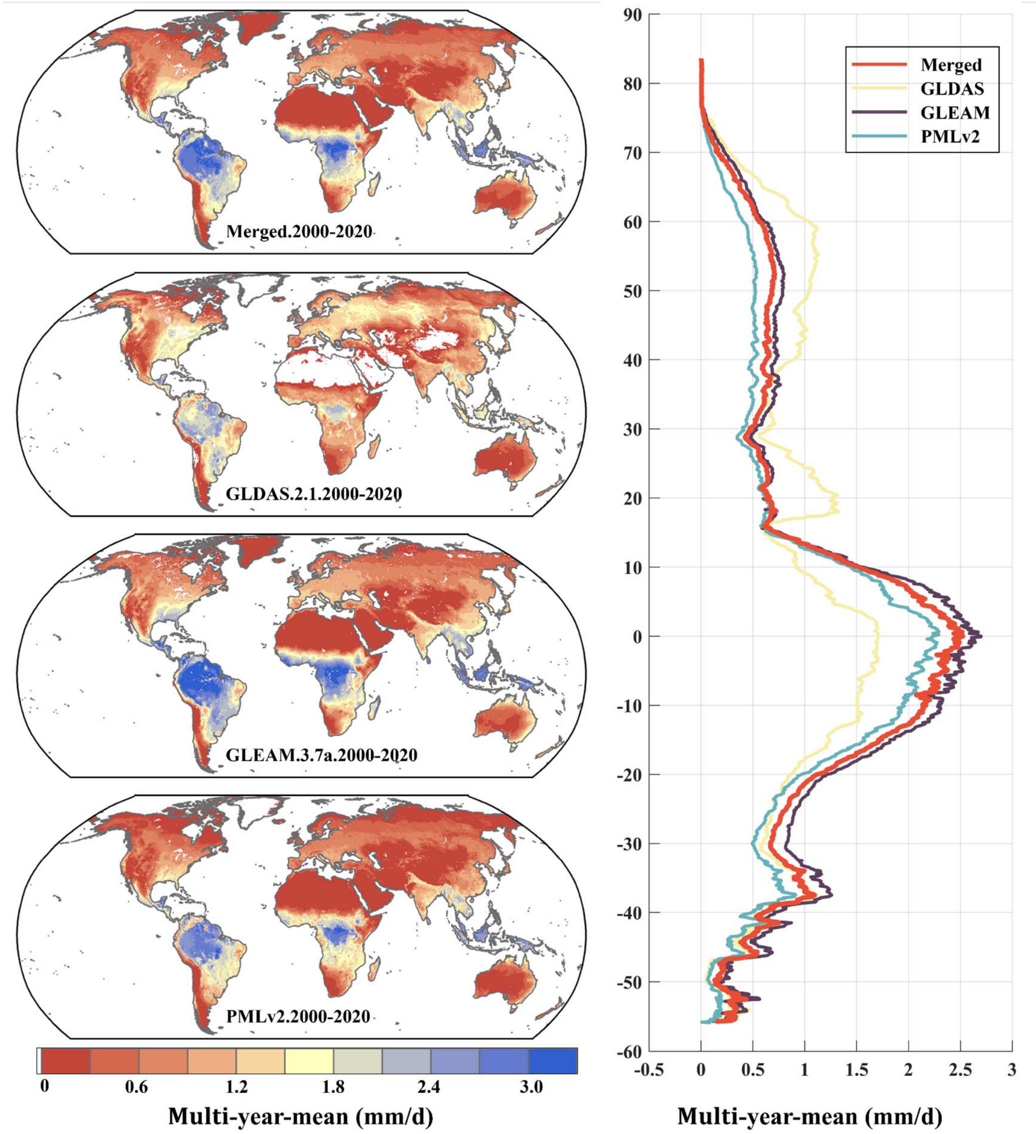

FIGURE.6 Global distribution of multi-year daily average transpiration at 0.1° for merged results, GLDAS, GLEAM and PMLv2, depicted alongside corresponding variation curves of average with latitude.

The results in Figure 6 indicated significant differences in the multi-year daily average distribution of global transpiration among different products, reaffirming the imperative need for data fusion. The multi-year daily transpiration results for different products were as follows (mean $\pm$ standard deviation): Merged result: 0.79$\pm$0.79 mm/day, GLEAM: 0.89$\pm$0.85 mm/day, GLDAS: 0.91$\pm$0.61 mm/day, and PMLv2: 0.68$\pm$0.75 mm/day.

Across varying products, long-term average transpiration exhibited relatively consistent variations with latitude, with the merged dataset generally tracking with PMLv2 and GLEAM. However, GLDAS exhibited notably diminished values in equatorial regions compared to other products, including the fused results. Spatial analysis further unveiled that GLDAS consistently provided the lowest estimates for transpiration in tropical regions among the various product sets. Conversely, GLDAS values appeared elevated near 20°N, a phenomenon potentially attributed to the absence of estimates for the Sahara Desert and the Arabian Peninsula. Consequently, this data gap increased means along this latitude relative to other products. A parallel overestimation by GLDAS was discernible near the 60°N latitude, with concurrent data gaps evident in Central Asia at this latitude.

In summary, the multi-year average transpiration data derived from the fused results demonstrated a reasonable alignment with spatial distribution patterns and latitude-related trends, highlighting the robustness of the fusion methodology in addressing discrepancies among different product sources.

5. Discussion

5.1. Improved Data Fusion with ECC Consideration

This study employed a collocation analysis-based multisource merging approach that considers non-zero ECC, a critical factor often overlooked in previous fusion methods (Xueying Li et al., 2023; Park et al., 2023). Our comparative analyses, encompassing both theoretical and empirical assessments, unequivocally demonstrate the profound impact of ECC inclusion on enhancing the reliability of merged data compared to the conventional TC method. Theoretical underpinnings of collocation analysis, which evaluate the similarity among triple or quadruple inputs through cross-correlation metrics, play an important role in quantifying product errors, particularly in the absence of ground truth. The presence of familiar sources of random errors among inputs can lead to undesirable interference (M. Tugrul Yilmaz & Crow, 2014), particularly in the context of multisource data weight calculations, resulting in heightened uncertainties.

Non-zero ECC conditions introduce more substantial bias in the results mainly due to two reasons: (1) they cannot be mitigated by rescaling; (2) they cannot be compensated even with equal magnitude for all inputs; and (3) they have been frequently reported in recent studies for various variables (A. Gruber et al., 2016; C. Li et al., 2018, 2022). Within our site-scale analysis, we compared merging techniques employing EIVD and TC methodologies (Figure 2 and Figure 3). The improvement in merging outcomes and the substantial reduction in product errors underscore the profound significance of considering ECC. It is worth noting that while this study assumed the existence of non-zero ECC conditions between GLEAM and GLDAS, it is plausible that non-zero ECC conditions also exist between other pairs. Consequently, we present the EIVD-based ECC results for various pairs, highlighting our findings' broader applicability and impact.

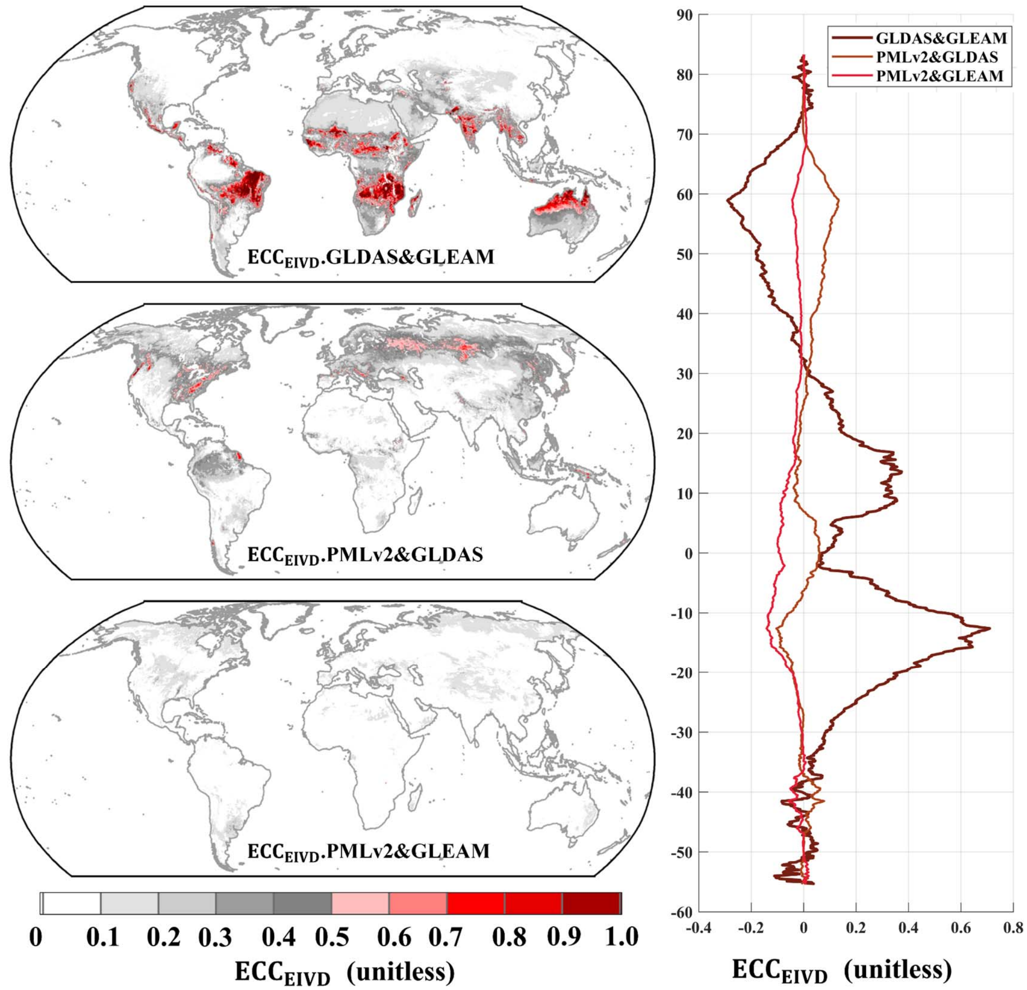

FIGURE.7 Global Distribution of estimated error cross-correlation (ECC) between GLDAS, GLEAM, and PMLv2 pairwise using EIVD alongside relevant variation curves of average with latitude.

As depicted in Figure 7, the ECC values of GLDAS and GLEAM were notably higher than those of PMLv2-GLDAS and PMLv2-GLEAM. The global average ECC values for different pairs were as follows (mean ± standard deviation): GLDAS-GLEAM: 0.22±0.30, PMLv2-GLEAM: 0.06±0.10, and PMLv2-GLDAS: 0.08±0.13. The results of the ECC indicated the presence of correlated random errors between GLEAM and GLDAS. These errors arose from the shared utilization of driving data, such as radiation and air temperature data sourced from ERA-Interim and ESA CCI SM v2.3 soil moisture data, contributing to the observed correlation between these two products. In contrast, ECC values for PMLv2 concerning GLDAS and GLEAM were relatively small. Some error correlation was noted between PMLv2 and GLDAS, likely due to using GLDAS2.0 data in the PMLv2 driver, while this study employed GLDAS2.1 data. Importantly, considering that the mean ECC between PMLv2 and GLDAS was less than 0.1, it can be reasonably inferred that this correlation had an insignificant impact on the results of the collocation analysis.

To summarize, the results of the ECC analysis supported the assumption of non-zero ECC between GLDAS and GLEAM in this study. This finding underlines the robustness of the random error variance in the products obtained through the EIVD methodology. In future research, incorporating more input datasets within an ECC fusion framework, along with a comprehensive evaluation of the strengths and weaknesses of different products, could lead to developing a more robust transpiration benchmark.

5.2. Potential uncertainty during data processing and evaluation

This study introduced two more potential sources of error. Firstly, data source errors arose from the statistical interpolation utilized for input data. Secondly, errors were associated with our analysis's partition methods employed as references.

We explained our approach in the Data and Methods sections, which involved downscaling the GLDAS and GLEAM datasets from 0.25° to 0.1° using statistical techniques. Additionally, we upscaled PMLv2 from 0.083° to 0.1° to ensure consistent spatial resolution across datasets. However, it is worth noting that our downscaling process did not incorporate supplementary information such as elevation, land cover changes, and other meteorological factors. Consequently, some errors in the statistical downscaling may exist compared to more intricate methodologies (Hernanz et al., 2023). Nevertheless, it is reassuring to highlight that our study yielded reliable transpiration estimates characterized by reasonable spatial patterns and consistent trends over multiple years. For future research endeavors, incorporating elevation and other pertinent data into the downscaling and upscaling procedures, possibly through methods like random forests, could offer potential enhancements in accuracy.

The sources of errors in our analysis were also linked to variations stemming from different partitioning methods. In our site-scale assessment of the fused results, we utilized mean transpiration values derived from three sets of ET partitioning methods as our reference benchmark. As outlined in the methodology section, these three methods exhibited some differences, particularly in their assumptions regarding specific conditions for T≈ET. Consequently, relying solely on the results from a single partitioning method as a reference would not have provided a sufficiently reliable basis for our evaluations (Xi Li et al., 2019). Therefore, we chose to use the average values as our reference standard. It is important to note that numerous other ET partitioning methods were available (Stoy et al., 2019), and in this study, we selected three commonly used ones. Utilizing results from alternative methods as references could have led to different conclusions.

5.3. Validation, Potential Applications, and Future Enhancements

In this study, our primary focus centered on site-scale validation against partitioned results from FLUXNET sites. However, with the continual advancement and increasing availability of sap flow observations, offering a more direct approach for assessing transpiration estimates, the integration of sap flow data holds significant promise for further enhancing our product's validation and overall quality. Notably, recent work by Bittencourt et al. (2023) successfully validated the reliability of GLEAM transpiration products utilizing SAPFLUXNET data (Poyatos et al., 2021). Their study introduced a data-processing approach, enabling SAPFLUXNET data as benchmarks. Nevertheless, it is essential to acknowledge that their findings also emphasized the inherent uncertainty in sap flow data. Therefore, we advocate for a comprehensive comparison between observed and estimated variations, as demonstrated in their study using Z-scores. In summary, we maintain that the site references chosen in this study were relatively robust. However, future investigations may consider exploring alternative reference sources to provide insights into potential disparities when incorporating sap flow data into the analysis.

Turning our attention to potential applications of our product, we propose three key avenues. (i) Global Transpiration Trends: Our product offers insights into current transpiration patterns and enables the examination of multi-year trends in global transpiration. Such long-term trends are essential in understanding how ecosystems respond to changing environmental conditions, especially in the context of a warming climate; (ii) Transpiration-to-Evapotranspiration Ratio: Beyond trends in global transpiration, our product provides another metric—the ratio of transpiration to evapotranspiration. Understanding variations in this ratio can lead to more efficient water resource management strategies and improved predictions of water availability in different regions; (iii) Attribution Analysis: Our product can serve as a valuable tool for attribution analysis, helping researchers identify the drivers behind transpiration patterns. This knowledge is vital for disentangling the roles of climate variability, land-use changes, and other factors in shaping terrestrial water fluxes.

We have outlined a proactive approach to future updates in our ongoing commitment to providing a robust and reliable transpiration product. First and foremost, we will rigorously validate and incorporate more reliable datasets into our fusion process. This validation ensures that the data sources we integrate meet high-quality standards. Furthermore, as the scientific community continually improves and updates input datasets, we are dedicated to promptly adapting our product to accommodate the latest versions. This agility ensures that our transpiration estimates remain up-to-date and reflect the most current scientific understanding.

6. Conclusion

Vegetation transpiration played a pivotal role in the terrestrial water cycle, and precise estimation became indispensable for comprehending and scrutinizing water cycle alterations. In this study, we applied the collocation analysis method, grounded in the EIVD approach that accounted for non-zero ECC conditions, to examine random error variances within three datasets: GLDAS, GLEAM, and PMLv2. Subsequently, we conducted data fusion to acquire global daily gridded transpiration data of 0.1° from 2000 to 2020. The primary findings of this investigation include:

1. The collocation analysis method can effectively be used for error analysis of global-scale transpiration products. The calculated random error variances can be used for further data fusion when considering the correlation of random errors in the products.
2. At the site scale, compared to the mean transpiration estimated by three commonly used ET partition methods as a reference, the fused product shows improved accuracy, especially a significant reduction in errors compared to the results of simple averaging and traditional TC fusion without considering non-zero ECC.
3. The fused results perform better than other products for different Plant Functional Types (PFTs). In some sites, PMLv2 exhibits superior performance, partly validated by its use of FLUXNET site data for calibration, supporting the reliability of the fused results.
4. Significant differences emerged among different products when examining the global multi-year average transpiration distribution. The fused results displayed a more reasonable distribution, closely resembling the distributions of PMLv2 and GLEAM. Nevertheless, some disparities were evident compared to GLDAS results, particularly in tropical regions.
5. When utilizing the error information derived from collocation analysis for merging, it is crucial to consider the potential presence of non-zero ECC. Comparing the merging schemes with and without considering non-zero ECC, it was found that considering ECC improves the accuracy of the merging process. Additionally, when using collocation analysis, it is necessary to identify which

products may have ECC in advance, providing more effective support for data merging and obtaining more accurate product error information.

In conclusion, our collocation-based data merging approach demonstrated promising potential for merging transpiration products. The resulting product exhibited good overall performance and met the requirements for more detailed research. Additional evaluation of the merged product in specific regions improved its accuracy. In future studies, dynamic weights were computed by considering suitable merging periods for different products to enhance the quality of the merged product, and more sophisticated combination schemes were explored to improve accuracy.

Author Contribution

C.L. conceived and designed the study, collected and analyzed the data, and wrote the manuscript. H.Y participated in the study design, provided intellectual insights, and reviewed the manuscript for important intellectual content. Z.T., J.H., and Z.L. guided the research process and critically reviewed the manuscript. All authors have read and approved the final version of the manuscript.

Competing interests

The authors declare that they have no conflict of interest.

Open Research

The datasets utilized in this research can be accessed through the links provided in the Dataset Section. The merged product is uploaded to Zenodo (Considering potential modifications during the review, we plan to upload after publication to minimize version changes). The data is distributed under a Creative Commons Attribution 4.0 License. Codes to apply the merging process and analyze the results will be available upon request.

Acknowledgments

This research was supported by the National Natural Science Foundation of China (grant no. 52309022 and 42041004) and the China National Key R&D Program (grant no. 2022YFC3002802).

Reference

Bates, J. M., & Granger, C. W. (1969). The combination of forecasts. *Journal of the Operational Research Society*, *20*(4), 451–468.

Bayat, B., Camacho, F., Nickeson, J., Cosh, M., Bolten, J., Vereecken, H., & Montzka, C. (2021). Toward operational validation systems for global satellite-based terrestrial essential climate variables. *International Journal of Applied Earth Observation and Geoinformation*, *95*. https://doi.org/10.1016/j.jag.2020.102240

Berg, A., & Sheffield, J. (2019). Evapotranspiration Partitioning in CMIP5 Models: Uncertainties and Future Projections. *Journal of Climate*, *32*(10), 2653–2671. https://doi.org/10.1175/JCLI-D-18-0583.1

Binks, O., Cernusak, L. A., Liddell, M., Bradford, M., Coughlin, I., Carle, H., et al. (2022). Forest system hydraulic conductance: partitioning tree and soil components. *New Phytol*, *233*(4), 1667–1681. https://doi.org/10.1111/nph.17895

Bittencourt, P., Rowland, L., Sitch, S., Poyatos, R., Miralles, D. G., & Mencuccini, M.

(2023). Bridging Scales: An Approach to Evaluate the Temporal Patterns of Global Transpiration Products Using Tree-Scale Sap Flow Data. *Journal of Geophysical Research: Biogeosciences*, *128*(3), e2022JG007308. https://doi.org/10.1029/2022JG007308

Bright, R. M., Miralles, D. G., Poyatos, R., & Eisner, S. (2022). Simple Models Outperform More Complex Big-Leaf Models of Daily Transpiration in Forested Biomes. *Geophysical Research Letters*, *49*(18), e2022GL100100. https://doi.org/10.1029/2022GL100100

Cowan, I. R., & GD, F. (1977). Stomatal function in relation to leaf metabolism and environment.

Deng, X., Zhu, L., Wang, H., Zhang, X., Tong, C., Li, S., & Wang, K. (2023). Triple Collocation Analysis and In Situ Validation of the CYGNSS Soil Moisture Product. *IEEE Journal of Selected Topics in Applied Earth Observations and Remote Sensing*, *16*, 1883–1899. https://doi.org/10.1109/jstars.2023.3235111

Dong, J., Crow, W. T., Duan, Z., Wei, L., & Lu, Y. (2019). A double instrumental variable method for geophysical product error estimation. *Remote Sensing of Environment*, *225*, 217–228. https://doi.org/10.1016/j.rse.2019.03.003

Dong, J., Wei, L., Chen, X., Duan, Z., & Lu, Y. (2020). An instrument variable based algorithm for estimating cross-correlated hydrological remote sensing errors. *Journal of Hydrology*, *581*, 124413. https://doi.org/10.1016/j.jhydrol.2019.124413

Dong, J., Crow, W. T., Chen, X., Tangdamrongsub, N., Gao, M., Sun, S., et al. (2022). Statistical uncertainty analysis-based precipitation merging (SUPER): A new framework for improved global precipitation estimation. *Remote Sensing of Environment*, *283*, 113299. https://doi.org/10.1016/j.rse.2022.113299

Fisher, J. B., Melton, F., Middleton, E., Hain, C., Anderson, M., Allen, R., et al. (2017). The future of evapotranspiration: Global requirements for ecosystem functioning, carbon and climate feedbacks, agricultural management, and water resources. *Water Resources Research*, *53*(4), 2618–2626. https://doi.org/10.1002/2016wr020175

Gruber, A., Su, C.-H., Zwieback, S., Crow, W., Dorigo, W., & Wagner, W. (2016). Recent advances in (soil moisture) triple collocation analysis. *International Journal of Applied Earth Observation and Geoinformation*, *45*, 200–211. https://doi.org/10.1016/j.jag.2015.09.002

Gruber, Alexander, Su, C., Crow, W. T., Zwieback, S., Dorigo, W., & Wagner, W. (2016). Estimating error cross-correlations in soil moisture data sets using extended collocation analysis. *Journal of Geophysical Research: Atmospheres*, *121*(3), 1208–1219.

Gruber, Alexander, Dorigo, W. A., Crow, W., & Wagner, W. (2017). Triple Collocation-Based Merging of Satellite Soil Moisture Retrievals. *IEEE Transactions on Geoscience and Remote Sensing*, *55*(12), 6780–6792. https://doi.org/10.1109/TGRS.2017.2734070

Gruber, Alexander, Scanlon, T., van der Schalie, R., Wagner, W., & Dorigo, W. (2019). Evolution of the ESA CCI Soil Moisture climate data records and their underlying merging methodology. *Earth System Science Data*, *11*(2), 717–739. https://doi.org/10.5194/essd-11-717-2019

Hernanz, A., Correa, C., Domínguez, M., Rodríguez-Guisado, E., & Rodríguez-Camino, E. (2023). Comparison of machine learning statistical downscaling and regional climate models for temperature, precipitation, wind speed, humidity and radiation over Europe under present conditions. *International Journal of Climatology*, joc.8190. https://doi.org/10.1002/joc.8190

Hoareau, N., Portabella, M., Lin, W., Ballabrera-Poy, J., & Turiel, A. (2018). Error characterization of sea surface salinity products using triple collocation analysis. *IEEE Transactions on Geoscience and Remote Sensing*, *56*(9), 5160–5168.

Jia, Y., Li, C., Yang, H., Yang, W., & Liu, Z. (2022). Assessments of three evapotranspiration products over China using extended triple collocation and water balance methods. *Journal of Hydrology*, *614*, 128594.

Jiang, C., Ryu, Y., Fang, H., Myneni, R., Claverie, M., & Zhu, Z. (2017). Inconsistencies of interannual variability and trends in long-term satellite leaf area index products. *Glob Chang Biol*, *23*(10), 4133–4146. https://doi.org/10.1111/gcb.13787

Keenan, T. F., Prentice, I. C., Canadell, J. G., Williams, C. A., Wang, H., Raupach, M., & Collatz, G. J. (2016). Recent pause in the growth rate of atmospheric CO2 due to enhanced terrestrial carbon uptake. *Nat Commun*, *7*, 13428. https://doi.org/10.1038/ncomms13428

Kim, S., Sharma, A., Liu, Y. Y., & Young, S. I. (2021). Rethinking satellite data merging: from averaging to SNR optimization. *IEEE Transactions on Geoscience and Remote Sensing*, *60*, 1–15.

Kling, H., Fuchs, M., & Paulin, M. (2012). Runoff conditions in the upper Danube basin under an ensemble of climate change scenarios. *Journal of Hydrology*, *424–425*, 264–277. https://doi.org/10.1016/j.jhydrol.2012.01.011

Knoben, W. J. M., Freer, J. E., & Woods, R. A. (2019). Technical note: Inherent benchmark or not? Comparing Nash–Sutcliffe and Kling–Gupta efficiency scores. *Hydrology and Earth System Sciences*, *23*(10), 4323–4331. https://doi.org/10.5194/hess-23-4323-2019

Leuning, R., Zhang, Y. Q., Rajaud, A., Cleugh, H., & Tu, K. (2009). Correction to "A simple surface conductance model to estimate regional evaporation using MODIS leaf area index and the Penman-Monteith equation." *Water Resources Research*, *45*(1). https://doi.org/10.1029/2008wr007631

Li, C., Tang, G., & Hong, Y. (2018). Cross-evaluation of ground-based, multi-satellite and reanalysis precipitation products: Applicability of the Triple Collocation method across Mainland China. *Journal of Hydrology*, *562*, 71–83. https://doi.org/10.1016/j.jhydrol.2018.04.039

Li, C., Yang, H., Yang, W., Liu, Z., Jia, Y., Li, S., & Yang, D. (2022). Error Characterization of Global Land Evapotranspiration Products: Collocation-based approach. *Journal of Hydrology*, 128102.

Li, C., Liu, Z., Tu, Z., Shen, J., He, Y., & Yang, H. (2023). Assessment of global gridded transpiration products using the extended instrumental variable technique (EIVD). *Journal of Hydrology*, *623*, 129880. https://doi.org/10.1016/j.jhydrol.2023.129880

Li, Xi, Gentine, P., Lin, C., Zhou, S., Sun, Z., Zheng, Y., et al. (2019). A simple and objective method to partition evapotranspiration into transpiration and evaporation at eddy-covariance sites. *Agricultural and Forest Meteorology*, *265*, 171–182. https://doi.org/10.1016/j.agrformet.2018.11.017

Li, Xueying, Zhang, W., Vermeulen, A., Dong, J., & Duan, Z. (2023). Triple collocation-based merging of multisource gridded evapotranspiration data in the Nordic Region. *Agricultural and Forest Meteorology*, *335*, 109451. https://doi.org/10.1016/j.agrformet.2023.109451

Lian, X., Piao, S., Huntingford, C., Li, Y., Zeng, Z., Wang, X., et al. (2018). Partitioning global land evapotranspiration using CMIP5 models constrained by observations. *Nature Climate Change*, *8*(7), 640–646. https://doi.org/10.1038/s41558-018-0207-9

Lin, C., Gentine, P., Huang, Y., Guan, K., Kimm, H., & Zhou, S. (2018). Diel ecosystem conductance response to vapor pressure deficit is suboptimal and independent of soil moisture. *Agricultural and Forest Meteorology*, *250*, 24–34.

Loveland, T. R., Zhu, Z., Ohlen, D. O., Brown, J. F., Reed, B. C., & Yang, L. (1999). An analysis of the IGBP global land-cover characterization process. *Photogrammetric Engineering and Remote Sensing*, *65*, 1021–1032.

Martens, B., Miralles, D. G., Lievens, H., van der Schalie, R., de Jeu, R. A. M., Fernández-Prieto, D., et al. (2017). GLEAM v3: satellite-based land evaporation and root-zone soil moisture. *Geoscientific Model Development*, *10*(5), 1903–1925. https://doi.org/10.5194/gmd-10-1903-2017

Mcgrath, J. M., & Lobell, D. B. (2013). Reduction of transpiration and altered nutrient allocation contribute to nutrient decline of crops grown in elevated CO2 concentrations. *Plant, Cell & Environment*, *36*(3), 697–705.

Ming, W., Ji, X., Zhang, M., Li, Y., Liu, C., Wang, Y., & Li, J. (2022). A Hybrid Triple Collocation-Deep Learning Approach for Improving Soil Moisture Estimation from Satellite and Model-Based Data. *Remote Sensing*, *14*(7). https://doi.org/10.3390/rs14071744

Miralles, D. G., Jiménez, C., Jung, M., Michel, D., Ershadi, A., McCabe, M. F., et al. (2016). The WACMOS-ET project – Part 2: Evaluation of global terrestrial evaporation data sets. *Hydrology and Earth System Sciences*, *20*(2), 823–842. https://doi.org/10.5194/hess-20-823-2016

Miralles, D Gonzalez, Holmes, T., De Jeu, R., Gash, J., Meesters, A., & Dolman, A.

(2011). Global land-surface evaporation estimated from satellite-based observations. *Hydrology and Earth System Sciences*, *15*(2), 453–469.

Miralles, Diego G, Van Den Berg, M. J., Gash, J. H., Parinussa, R. M., De Jeu, R. A., Beck, H. E., et al. (2014). El Niño–La Niña cycle and recent trends in continental evaporation. *Nature Climate Change*, *4*(2), 122–126.

Nelson, J. A., Perez-Priego, O., Zhou, S., Poyatos, R., Zhang, Y., Blanken, P. D., et al. (2020). Ecosystem transpiration and evaporation: Insights from three water flux partitioning methods across FLUXNET sites. *Glob Chang Biol*, *26*(12), 6916–6930. https://doi.org/10.1111/gcb.15314

Nelson, Jacob A, Carvalhais, N., Cuntz, M., Delpierre, N., Knauer, J., Ogée, J., et al. (2018). Coupling Water and Carbon Fluxes to Constrain Estimates of Transpiration: The TEA Algorithm. *Journal of Geophysical Research: Biogeosciences*, *123*(12), 3617–3632. https://doi.org/10.1029/2018jg004727

Oogathoo, S., Houle, D., Duchesne, L., & Kneeshaw, D. (2022). Tree transpiration well simulated by the Canadian Land Surface Scheme (CLASS) but not during drought. *Journal of Hydrology*, *604*. https://doi.org/10.1016/j.jhydrol.2021.127196

Park, J., Baik, J., & Choi, M. (2023). Triple collocation-based multisource evaporation and transpiration merging. *Agricultural and Forest Meteorology*, *331*, 109353.

Pastorello, G., Trotta, C., Canfora, E., Chu, H., Christianson, D., Cheah, Y. W., et al.

(2020). The FLUXNET2015 dataset and the ONEFlux processing pipeline for eddy covariance data. *Sci Data*, *7*(1), 225. https://doi.org/10.1038/s41597-020-0534-3

Perez-Priego, O., Katul, G., Reichstein, M., El-Madany, T. S., Ahrens, B., Carrara, A., et al. (2018). Partitioning Eddy Covariance Water Flux Components Using Physiological and Micrometeorological Approaches. *Journal of Geophysical Research: Biogeosciences*, *123*(10), 3353–3370. https://doi.org/10.1029/2018jg004637

Poyatos, R., Granda, V., Flo, V., Adams, M. A., Adorján, B., Aguadé, D., et al. (2021). Global transpiration data from sap flow measurements: the SAPFLUXNET database. *Earth System Science Data*, *13*(6), 2607–2649. https://doi.org/10.5194/essd-13-2607-2021

Priestley, C. H. B., & TAYLOR, R. J. (1972). On the assessment of surface heat flux and evaporation using large-scale parameters. *Monthly Weather Review*, *100*(2), 81–92.

Ribal, A., & Young, I. R. (2020). Global Calibration and Error Estimation of Altimeter, Scatterometer, and Radiometer Wind Speed Using Triple Collocation. *Remote Sensing*, *12*(12). https://doi.org/10.3390/rs12121997

Rodell, M., Famiglietti, J., Chen, J., Seneviratne, S., Viterbo, P., Holl, S., & Wilson, C. (2004). Basin scale estimates of evapotranspiration using GRACE and other observations. *Geophysical Research Letters*, *31*(20).

Stoffelen, A. (1998). Toward the true near-surface wind speed: Error modeling and calibration using triple collocation. *Journal of Geophysical Research: Oceans*, *103*(C4), 7755–7766. https://doi.org/10.1029/97jc03180

Stoy, P. C., El-Madany, T. S., Fisher, J. B., Gentine, P., Gerken, T., Good, S. P., et al. (2019). Reviews and syntheses: Turning the challenges of partitioning ecosystem evaporation and transpiration into opportunities. *Biogeosciences*, *16*(19), 3747–3775.

Su, C.-H., Ryu, D., Crow, W. T., & Western, A. W. (2014). Beyond triple collocation: Applications to soil moisture monitoring. *Journal of Geophysical Research: Atmospheres*, *119*(11), 6419–6439. https://doi.org/10.1002/2013jd021043

Sun, J., McColl, K. A., Wang, Y., Rigden, A. J., Lu, H., Yang, K., et al. (2021). Global evaluation of terrestrial near-surface air temperature and specific humidity retrievals from the Atmospheric Infrared Sounder (AIRS). *Remote Sensing of Environment*, *252*. https://doi.org/10.1016/j.rse.2020.112146

Talsma, C. J., Good, S. P., Jimenez, C., Martens, B., Fisher, J. B., Miralles, D. G., et al. (2018). Partitioning of evapotranspiration in remote sensing-based models. *Agricultural and Forest Meteorology*, *260–261*, 131–143. https://doi.org/10.1016/j.agrformet.2018.05.010

Towner, J., Cloke, H. L., Zsoter, E., Flamig, Z., Hoch, J. M., Bazo, J., et al. (2019). Assessing the performance of global hydrological models for capturing peak river flows in the Amazon basin. *Hydrology and Earth System Sciences*, *23*(7), 3057–3080. https://doi.org/10.5194/hess-23-3057-2019

Vogelzang, J., Stoffelen, A., & Verhoef, A. (2022). The Effect of Error Non-Orthogonality on Triple Collocation Analyses. *Remote Sensing*, *14*(17), 4268.

Wei, Z., Yoshimura, K., Wang, L., Miralles, D. G., Jasechko, S., & Lee, X. (2017). Revisiting the contribution of transpiration to global terrestrial evapotranspiration. *Geophysical Research Letters*, *44*(6), 2792–2801. https://doi.org/10.1002/2016gl072235

Wu, K., Ryu, D., Nie, L., & Shu, H. (2021). Time-variant error characterization of SMAP and ASCAT soil moisture using Triple Collocation Analysis. *Remote Sensing of Environment*, *256*. https://doi.org/10.1016/j.rse.2021.112324

Yang, S., Zhao, B., Yang, D., Wang, T., Yang, Y., Ma, T., & Santisirisomboon, J. (2023). Future changes in water resources, floods and droughts under the joint impact of climate and land-use changes in the Chao Phraya basin, Thailand. *Journal of Hydrology*, *620*. https://doi.org/10.1016/j.jhydrol.2023.129454

Yilmaz, M. T., Crow, W. T., Anderson, M. C., & Hain, C. (2012). An objective methodology for merging satellite- and model-based soil moisture products. *Water Resources Research*, *48*(11), n/a-n/a. https://doi.org/10.1029/2011wr011682

Yilmaz, M. Tugrul, & Crow, W. T. (2014). Evaluation of Assumptions in Soil Moisture Triple Collocation Analysis. *Journal of Hydrometeorology*, *15*(3), 1293–1302. https://doi.org/10.1175/JHM-D-13-0158.1

Yin, G., & Park, J. (2021). The use of triple collocation approach to merge satellite- and model-based terrestrial water storage for flood potential analysis. *Journal of Hydrology*, *603*. https://doi.org/10.1016/j.jhydrol.2021.127197

Zhang, Y., Kong, D., Gan, R., Chiew, F. H. S., McVicar, T. R., Zhang, Q., & Yang, Y. (2019). Coupled estimation of 500 m and 8-day resolution global evapotranspiration and gross primary production in 2002–2017. *Remote Sensing of Environment*, *222*, 165–182. https://doi.org/10.1016/j.rse.2018.12.031

Zhou, S., Yu, B., Zhang, Y., Huang, Y., & Wang, G. (2016). Partitioning evapotranspiration based on the concept of underlying water use efficiency. *Water Resources Research*, *52*(2), 1160–1175. https://doi.org/10.1002/2015wr017766

Zou, A., Gupta, M., & Maroo, S. C. (2020). Transpiration mechanism in confined nanopores. *The Journal of Physical Chemistry Letters*, *11*(9), 3637–3641.

Figure1.

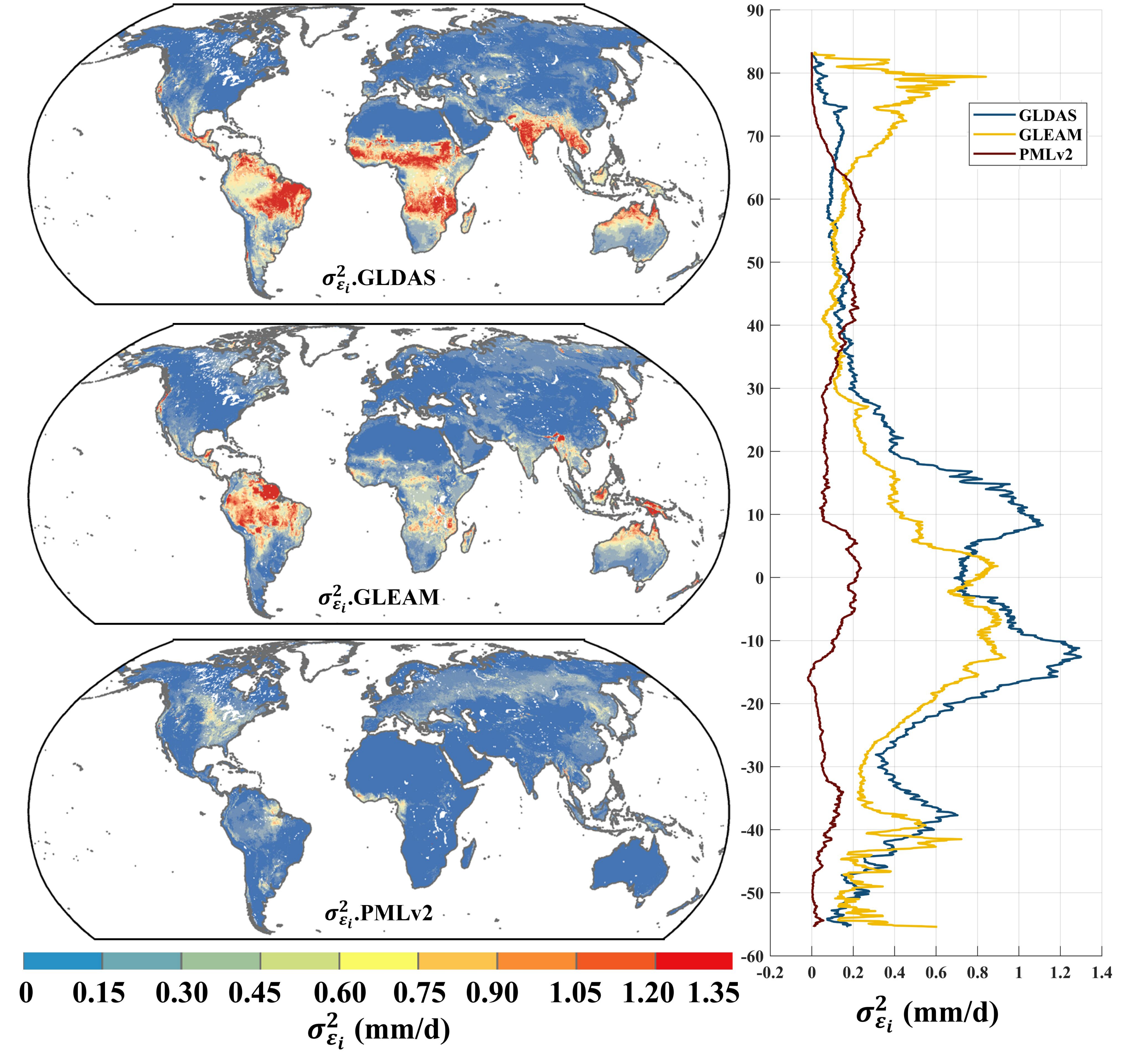

$\sigma^2_{\varepsilon_i}$.GLDAS
$\sigma^2_{\varepsilon_i}$.GLEAM
$\sigma^2_{\varepsilon_i}$.PMLv2
0 0.15 0.30 0.45 0.60 0.75 0.90 1.05 1.20 1.35
$\sigma^2_{\varepsilon_i}$ (mm/d)
GLDAS
GLEAM
PMLv2
90 80 70 60 50 40 30 20 10 0 -10 -20 -30 -40 -50 -60
-0.2 0 0.2 0.4 0.6 0.8 1 1.2 1.4
$\sigma^2_{\varepsilon_i}$ (mm/d)

Figure2.

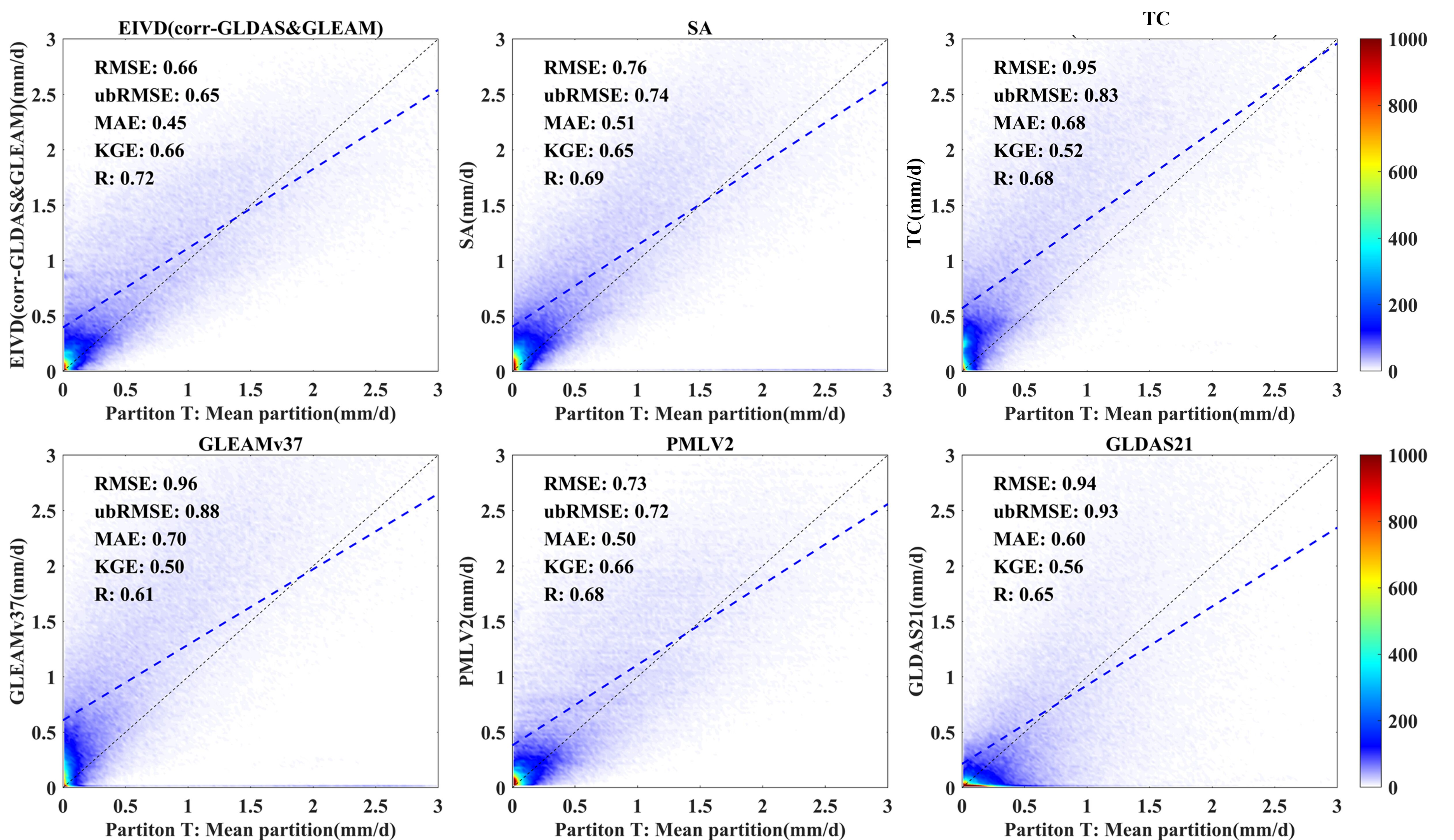

EIVD(corr-GLDAS&GLEAM)
RMSE: 0.66
ubRMSE: 0.65
MAE: 0.45
KGE: 0.66
R: 0.72
EIVD(corr-GLDAS&GLEAM)(mm/d)
Partiton T: Mean partition(mm/d)
SA
RMSE: 0.76
ubRMSE: 0.74
MAE: 0.51
KGE: 0.65
R: 0.69
SA(mm/d)
Partiton T: Mean partition(mm/d)
TC
RMSE: 0.95
ubRMSE: 0.83
MAE: 0.68
KGE: 0.52
R: 0.68
TC(mm/d)
Partiton T: Mean partition(mm/d)
GLEAMv37
RMSE: 0.96
ubRMSE: 0.88
MAE: 0.70
KGE: 0.50
R: 0.61
GLEAMv37(mm/d)
Partiton T: Mean partition(mm/d)
PMLV2
RMSE: 0.73
ubRMSE: 0.72
MAE: 0.50
KGE: 0.66
R: 0.68
PMLV2(mm/d)
Partiton T: Mean partition(mm/d)
GLDAS21
RMSE: 0.94
ubRMSE: 0.93
MAE: 0.60
KGE: 0.56
R: 0.65
GLDAS21(mm/d)
Partiton T: Mean partition(mm/d)

Figure3.

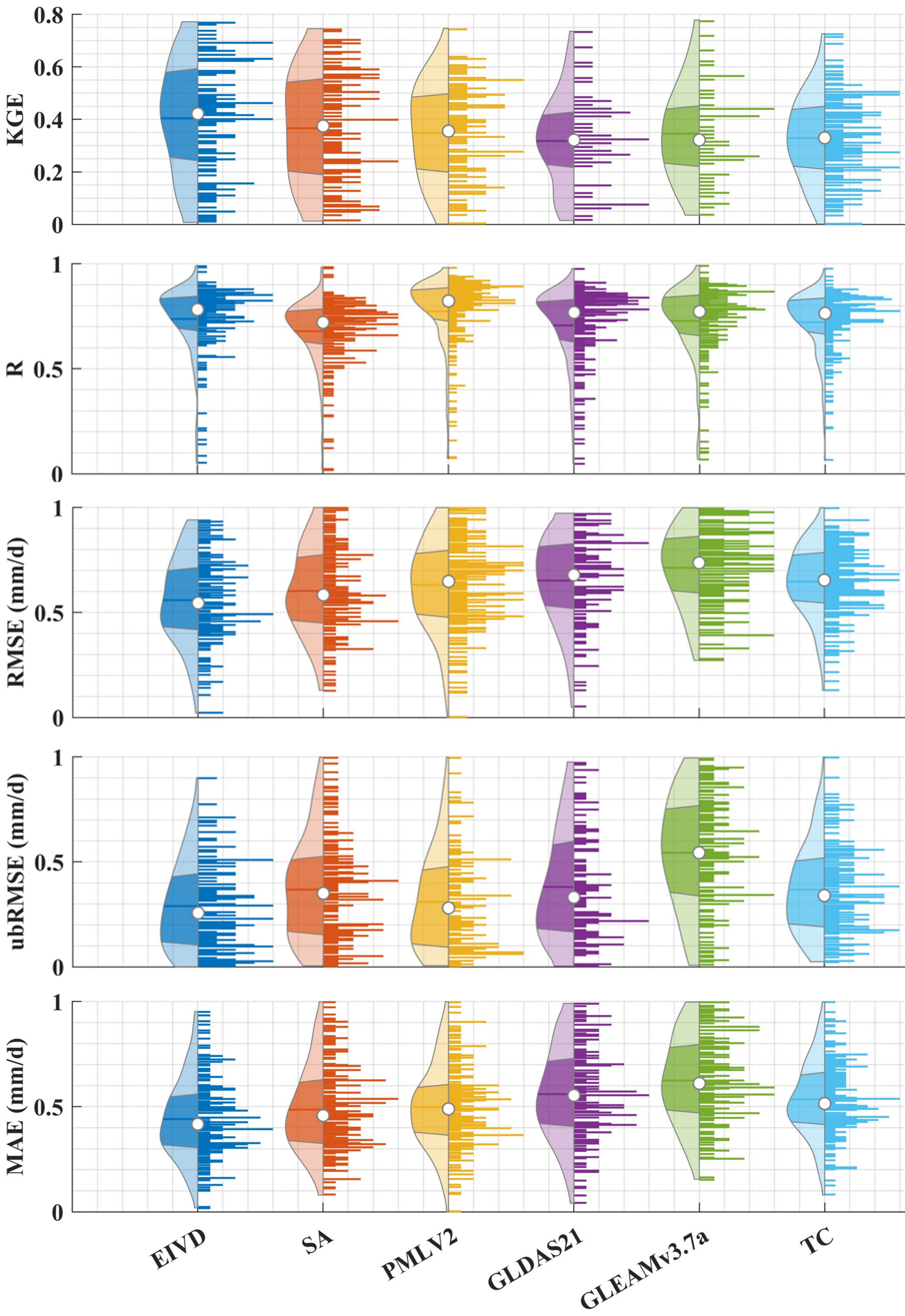

KGE
0.8
0.6
0.4
0.2
0
R
1
0.5
0
RMSE (mm/d)
1
0.5
0
ubRMSE (mm/d)
1
0.5
0
MAE (mm/d)
1
0.5
0
EIVD
SA
PMLV2
GLDAS21
GLEAMv3.7a
TC

Figure4.

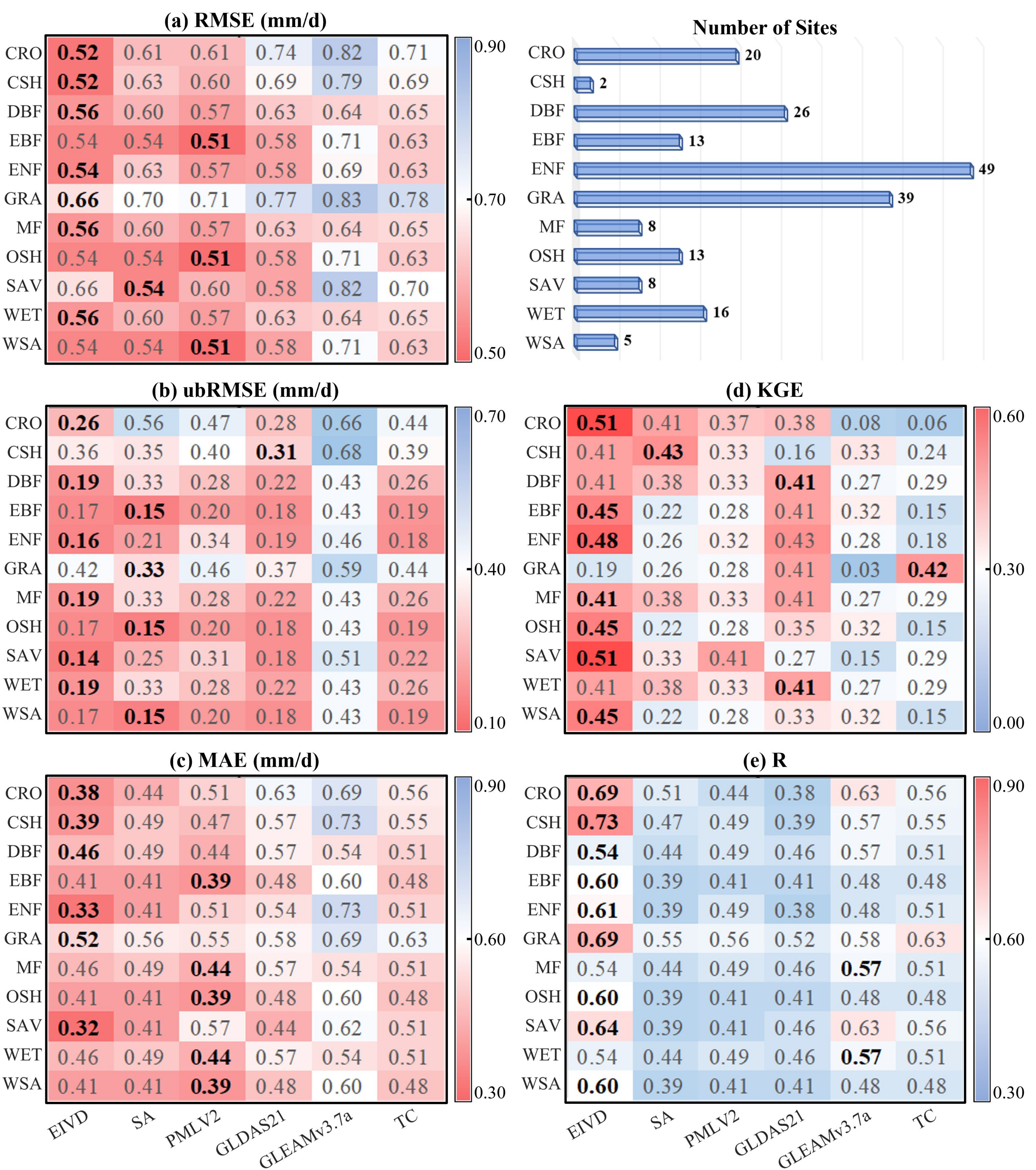

(a) RMSE (mm/d)
Number of Sites
(b) ubRMSE (mm/d)
(d) KGE
(c) MAE (mm/d)
(e) R
CRO
CSH
DBF
EBF
ENF
GRA
MF
OSH
SAV
WET
WSA
EIVD
SA
PMLV2
GLDAS21
GLEAMv3.7a
TC

Figure5.

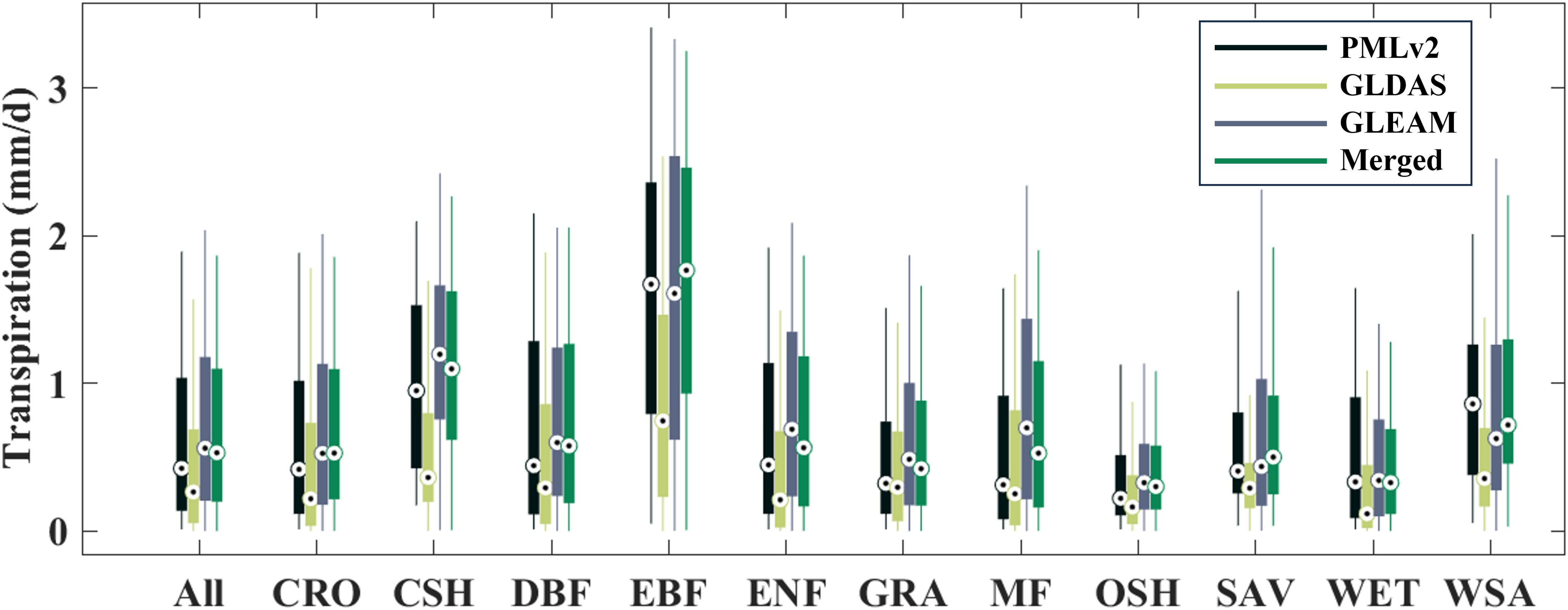
PMLv2
GLDAS
GLEAM
Merged
Transpiration (mm/d)
0
1
2
3
All
CRO
CSH
DBF
EBF
ENF
GRA
MF
OSH
SAV
WET
WSA

Figure6.

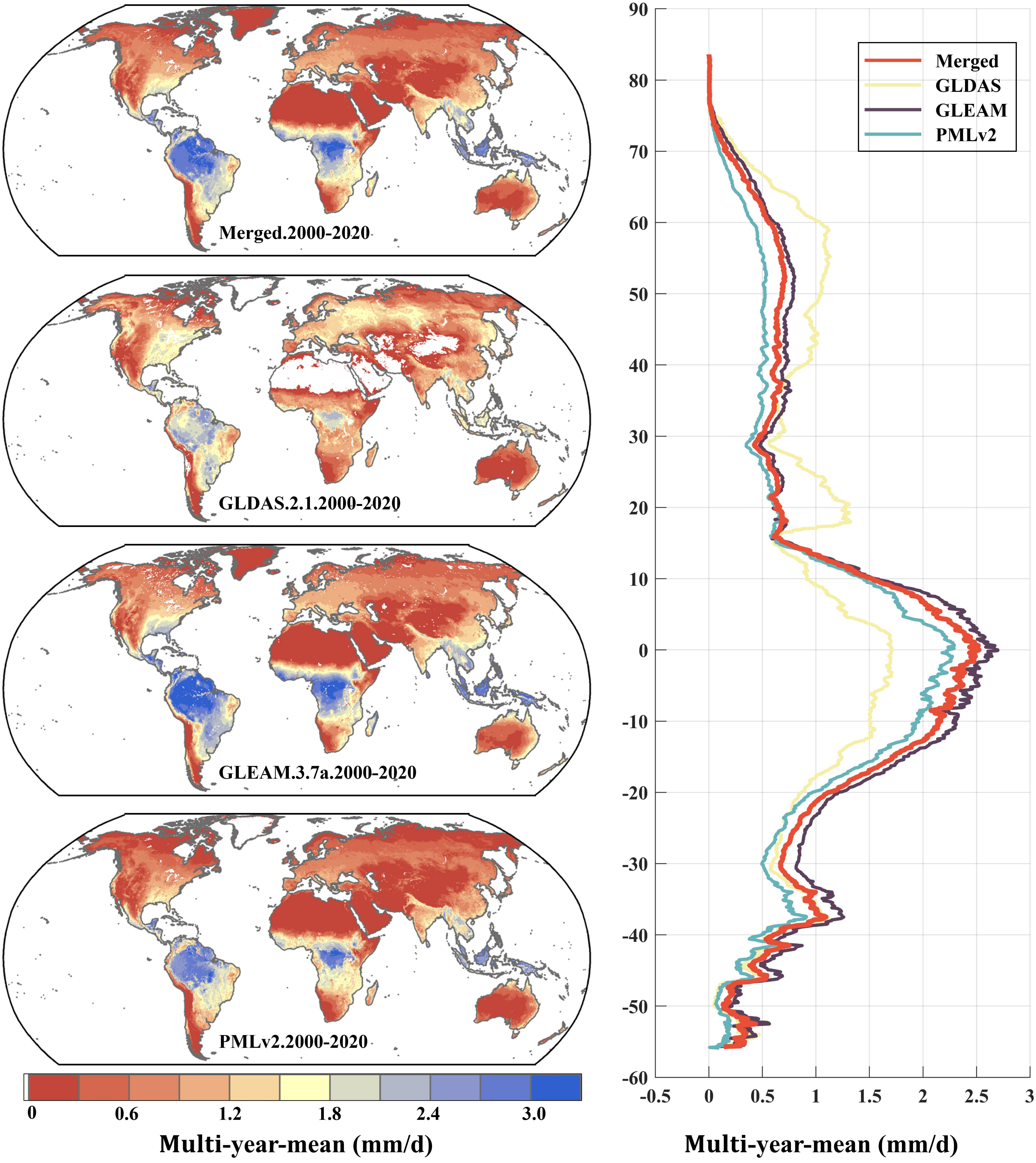

Merged.2000-2020
GLDAS.2.1.2000-2020
GLEAM.3.7a.2000-2020
PMLv2.2000-2020
0
0.6
1.2
1.8
2.4
3.0
Multi-year-mean (mm/d)
Merged
GLDAS
GLEAM
PMLv2
90
80
70
60
50
40
30
20
10
0
-10
-20
-30
-40
-50
-60
-0.5
0
0.5
1
1.5
2
2.5
3
Multi-year-mean (mm/d)

Figure7.

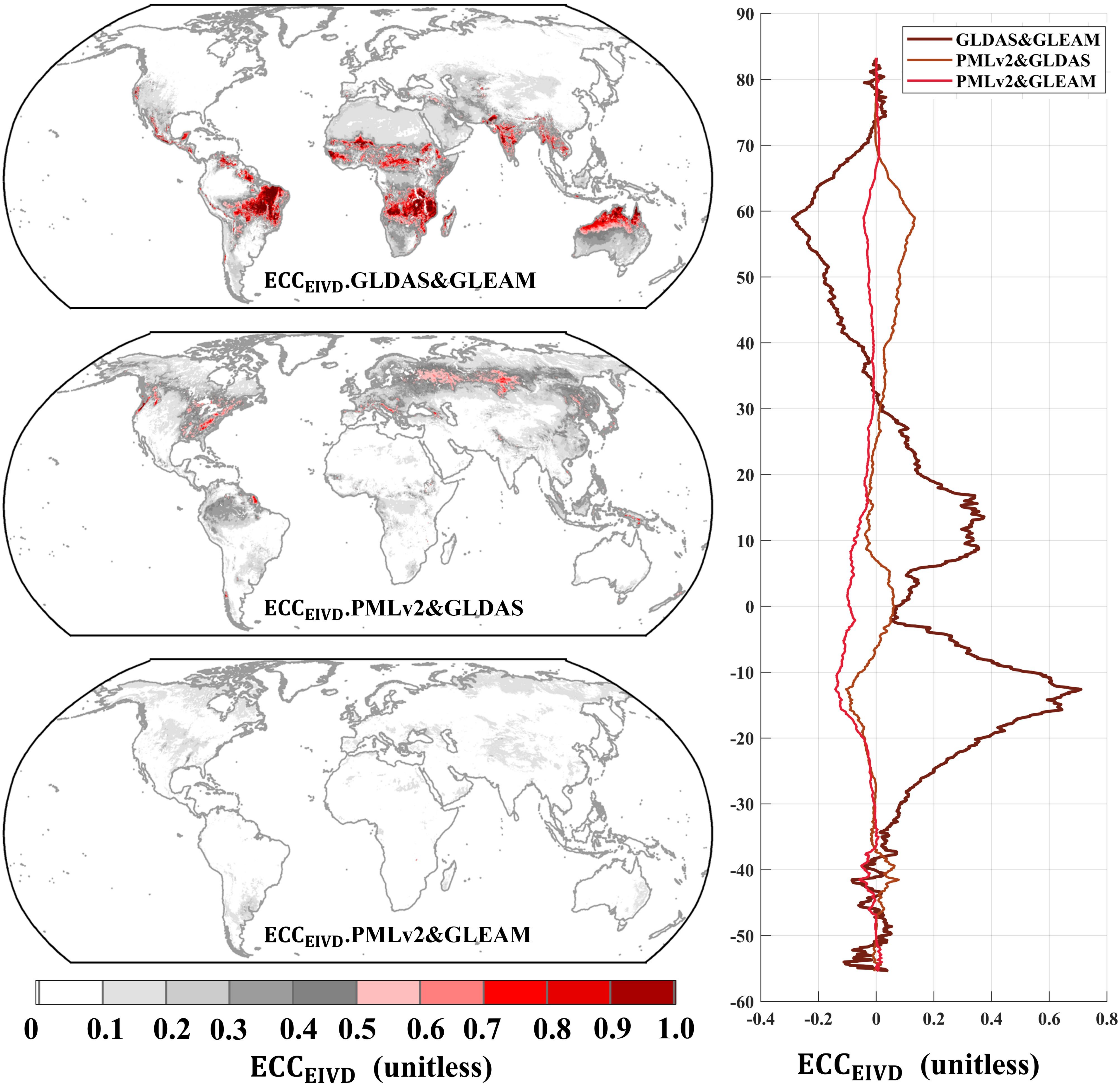

ECC$_{EIVD}$.GLDAS&GLEAM
ECC$_{EIVD}$.PMLv2&GLDAS
ECC$_{EIVD}$.PMLv2&GLEAM
0 0.1 0.2 0.3 0.4 0.5 0.6 0.7 0.8 0.9 1.0
ECC$_{EIVD}$ (unitless)
GLDAS&GLEAM
PMLv2&GLDAS
PMLv2&GLEAM
90 80 70 60 50 40 30 20 10 0 -10 -20 -30 -40 -50 -60
-0.4 -0.2 0 0.2 0.4 0.6 0.8
ECC$_{EIVD}$ (unitless)